Engineering Physics Bachelor Thesis

Breaking of the excitatory-inhibitory balance in neural networks

Author: Cristina Pericas Iturriagagoitia[2]

Director: Alex D. Reyes[1]

Co-director: Antonio Javier Pons[3]

New York University – Center for Neural Science[1]

Universitat Politècnica de Catalunya –

Escola Tècnica Superior d'Enginyeria de Telecomunicacions de Barcelona[2]

Escola Superior d'Enginyeries Industrial, Aerospacial i Audiovisual de Terrassa[3]

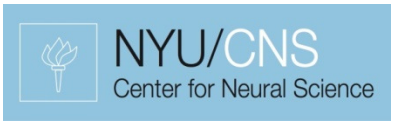

Acknowledgements

Foremost, I would like to express my sincere gratitude to Alex Reyes, without whom this work and my New York experience would have been impossible. He blindly offered me to join his laboratory and introduced me to the world of neuroscience. He has wisely guided, counseled and encouraged me through the entire project. His persistent enthusiasm and optimism are only two of the traits that make him such an exceptional tutor.

I also want to thank Jérémie Barral for his patience during my early days as a neuroscience experimentalist, for allowing me to use the set-up he had minutely put together and for always having a solution to every problem.

Further, I want to thank Antoni Pons, for believing in me and for his abroad tutoring. I would also like to mention the great support I have received from the administrative staff from both the New York University and the Universitat Politècnica de Catalunya.

Last but not least, I would like to thank my family and friends for encouraging me during this never-to-be-forgotten experience and for providing me with their occasional (but necessary) self-esteem-rising doses.

Abstract

A salient feature of neural networks is the maintenance of a balance between excitation and inhibition. This trait is crucial for rapid transmission of information as well as for preventing runaway excitation during, for example, epileptic seizures. There are, however, spontaneous events where this balance appears to be broken. Previous theoretical and experimental studies reveal the emergence of spontaneous population-wide intermittent bursts of coordinated neural activity interrupting asynchronous dynamics. Assuming population bursts are due to transient imbalances between excitation and inhibition, we combined computer simulations with electrophysiological recordings on live neurons in cultures to measure the variables responsible for this synchrony. Our results suggest that the bursts' properties are determined by those of the network, as highly dense and clustered cultures exhibit bursting behaviors while others do not. Moreover, we provide preliminary evidence that bursts may be generated locally within a region of the network where the balance of excitation and inhibition first breaks.

Keywords: excitatory-inhibitory balance, asynchronous dynamics, population bursts, electrophysiological recordings, cultures of neurons.

Table of contents

Introduction

The neural cortex is composed of recurrent coupled networks of excitatory (E) and inhibitory (I) neurons which interact strongly through local synaptic circuits[10]. The functionality of a synapse is generally defined upon whether the activation of a presynaptic action potential causes a positive (E) or a negative (I) deflection on the postsynaptic potential[21,38]. In other words, E neurons drag the membrane potential towards its firing threshold, whereas I lower the likelihood for the neuron to fire.

In neurophysiology, the concept of excitatory-inhibitory balance refers to the relative contributions of each type of synaptic inputs during a neuronal event. While inhibitory neurons are known to comprise less than the 25% of the population of cortical neurons[2,27], it is believed they play an important role in counterbalancing excitation. There are certain conditions where an excess of excitation is beneficial during, for example, sensory stimuli[15,36]. On the other hand, abnormally excessive excitatory activity in neural networks is known to be at the origin of epileptic seizures[6] and neuropathologies.

Classical theory of balanced networks

Over the past decade, numerous studies have provided strong evidence for closely balanced E and I. Early models on sparsely connected recurrent networks conjecture that this proportionality emerges naturally and is necessary in order for synaptic variability to be high and the cells not to remain in an inactive or abnormally saturated state[39]. This hypothesis is supported by experiments. *In vitro* electrophysiological recordings suggest that balance occurs due to the close and fast tracking of inhibition upon excitation[4,11,27,31,36,42]. Furthermore, *in vivo* experiments showed the spiking activity of I neurons is timed to balance E and plays an important role in damping excitation[10,27]. An important consequence of this balance is that an asynchronous state[5,11,31,43] is obtained with near-zero pairwise correlations of the membrane potentials.

Evidences of excitatory-inhibitory imbalance

However, balance is not always maintained and theoretical studies speculate that neurons sharing a great amount of inputs can occasionally synchronize their spiking patterns[37] which may be important for propagating

precise action potentials through cortical layers[7]. In the same vein, gain mechanisms that shift the balance towards overriding excitatory activity arise during sensory stimuli[15]: inhibition becomes slower and adapts more than excitation.

Previous measurements of the Reyes group on spontaneously active slices of auditory cortex[11,28,29,] show evidence of intermittent population-wide bursts of synchronized activity interrupting asynchronous cortical dynamics. Population bursts can be defined as brief but prominent irregular epochs of generalized spiking activity and neural depolarization[24,27]. The emergence of self-sustained collective dynamics like population bursts are indicative of network-wide correlated activity[35] and reflect the underlying functional architecture of recurrent circuitry[4,24,37,42]. Unfortunately, the classical theory of balanced networks is unable to reproduce population bursts[31].

Objectives and outline

Our aim is to get an insight on the possible mechanisms at the origin of breaking the E-I balance in recurrent networks. Our hypothesis are: 1) the bursts originate from a group or cluster of neurons in the network where E/I imbalance and bursts first occur, which then spread throughout the network; 2) the bursts vary with the density or number of neurons in the network. We based our analysis upon the fact that population-wide bursts are due to transient imbalances between E and I. To test these hypotheses, we use a combination of computer simulations and electrophysiological recordings in live neurons in cultures.

This thesis is divided into 5 chapters. First, I will give a brief review of spiking neuron models that give rise to the diverse spiking patterns. Then, after a short description of the experimental methods, I will describe *in vitro* electrophysiological recordings in cultures of cortical neurons[2] during spontaneous and optogenetic stimulation in order to measure the variables underlying burst generation and E-I imbalance. Finally, I will incorporate the experimental data into a numerical computer simulation of a neural network that consists of coupled E and I neurons, in order to elucidate the mechanisms for breaking the E-I balance.

Chapter 1

Spiking neuron models

Through a mathematical description of the biological properties of neurons, spiking neuron models aim to elucidate the mechanisms at the origin of the dynamics of the central nervous system[38]. Unfortunately, because of computational time, it is often necessary to compromise between computational simplicity and biological accuracy[18]. To simplify the models in a principled manner, we first examine single-compartment membrane voltage models and compare the results to more biologically realistic Hodgkin-Huxley models. While the simple models are used for the network simulations, the Hodgkin-Huxley models are useful for interpreting some of the experimental results in Chapter 3.

1.1 The neuron as an electronic circuit

Neurons are cells highly specialized for generating electric signals in response to chemical or sensory inputs and transmitting them to other cells[20]. Neurons have a soma (cell body), dendritic trees and an axon. Dendrites can receive up to a thousand inputs from other cells and axons transmit the neuronal signal to other dendrites across synapses[21]. As a result of the depolarization of the membrane above a threshold, neurons actively fire action potentials in an *all-or-nothing* fashion. The action potentials then propagate to other parts of the brain through the axon.

1.1.1. Equivalent circuit

It is a typical assumption to model the neural membrane as an electronic circuit driven by an external current and consisting on a capacitance and a set of time and voltage-dependent parallel conductances (Fig. 1.1). The neural membrane is a lipid bilayer impermeable to most charged particles[20]. It acts as a capacitor and separates ions along its interior and exterior surfaces. The intracellular potential is approximately -70 mV lower than the extracellular. The passive channels account for the membrane resistance R_m or alternatively the leakage conductance g_L ($=1/R_m$). The membrane time constant $\tau_m = R_m C_m$ is often used to characterize the time scale of the neuron's passive response to changes in its input[38].

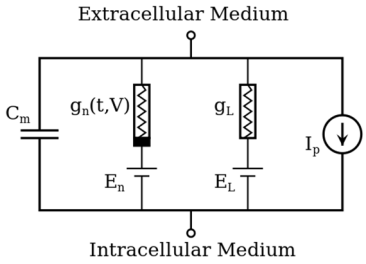

Figure 1.1. Electrical equivalent circuit of a neuronal membrane. Intra and extracellular mediums are separated by the cell membrane, modeled as an electrical circuit of parallel impedances.

Neural membranes have a wide variety of voltage-dependent selective ion channels that control the flow of ions across the membrane and are responsible for active-state dynamics. A time and voltage dependent conductance $g_n(t,V_m)$ accounts for the dynamics of such channels. Additionally, a synaptic conductance can be included in this term to account for synaptic inputs.

1.1.2. Total current through the cell membrane

The total current through the neuron's membrane is the sum of the currents due to the different types of channels, the synaptic inputs and the external stimulus. The dependence of the membrane potential with time is implicit in all of the equations.

$$C_m \frac{dV_m}{dt} = I_{ext}(t) + I_{leakage}(t) + I_{ions}(t) + I_{syn}(t) \tag{1.1}$$

Conductance-based models associate a conductance g_j and reversal potential V_j to each contribution of the current, the total resulting from the algebraic sum of conductance-driving force products.

$$I_{tot} = \sum_{j}^{K} g_j (V - V_j) \tag{1.2}$$

Synapses will also be described by conductance-based currents, their reversal potential being above the threshold for E (V_e=0mV) or below it for I (V_i=-80mV).

1.1.3. The synaptic current

The majority of neurons are bombarded by thousands of synaptic inputs coming from the presynaptic cells to which they are connected[36,43].

Immediately after the arrival of an action potential at the presynaptic terminal, neurotransmitters are released and bind to postsynaptic receptors, causing a change in the membrane's conductance for one of more ions. The consequent excitatory or inhibitory postsynaptic current (EPSC/IPSC; see eq. 1.2) into the cell membrane evokes a positive or negative deflection of the postsynaptic potential with respect to its resting value. From now on, we will refer as those as excitatory postsynaptic potentials (EPSPs; Fig. 1.2C green) and inhibitory postsynaptic potentials (IPSPs; Fig. 1.2C red).

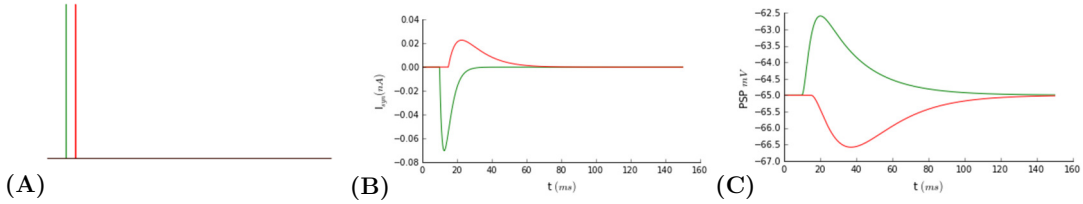

Figure 1.2. Synaptic transmission of an action potential. All amplitudes correspond to the ones used in the computational model in Chapter 5. **A**. Spikes at an excitatory (green) and inhibitory (red) presynaptic neuron. **B**. Evoked EPSC and IPSC. **C**. Evoked EPSP and IPSP. A convention establishes the EPSC current to be defined as negative, causing a depolarization of the cell, and the IPSC to be positive.

The alpha-function[13,16,25,33,38] (eq. 1.3) may be used to describe a synaptic conductance with finite duration of its rising phase and correlated rising and decay time courses. The total E and I changes in the postsynaptic conductance is the algebraic sum of time-shifted alpha-functions over all the spike times of the presynaptic cell.

$$g_j(t) = \begin{cases} g_{0_j} \dfrac{t}{\tau_j} e^{\frac{t}{\tau_j}} & t \geq 0 \\ 0 & otherwise \end{cases} \quad , \quad j=\{e,i\} \tag{1.3}$$

1.2 The leaky integrate-and-fire (LIF) model

Although ion flows are responsible for the generation of action potentials, there are simpler models that do not include those mechanisms. The integrate-and-fire model (Lapicque, 1907) only studies subthreshold voltages, while spiking activity is modelled by a reset condition activated whenever the potential reaches a threshold. These models are widely used for studying the response of a neuron to a large number of inputs or to study the dynamics within a neural network of interconnected cells due to their computational simplicity[32,38].

1.2.1. LIF master equation

LIF models the subthreshold dynamics of the neuron as those of a typical RC circuit. Passive membrane dynamics rely on the membrane capacitance C_m and the leakage time-independent conductance is responsible for the resting membrane potential[43] (see Section S1 of the Supplementary material).

$$C_m \frac{dV_m}{dt} = I_{ext}(t) - g_L(V - V_L) \tag{1.4}$$

In a more realistic situation, like the one we model in Chapter 5, integrate-and-fire neurons are part of a larger network where the input current is mainly due to the activity of presynaptic neurons. A synaptic input current (eq. 1.2) will then be added to the LIF master equation.

1.2.2. Membrane potential response to input currents

In this chapter, we want to describe the voltage response of a LIF to different inputs. These inputs could either represent an external stimulation or synaptic E and I inputs.

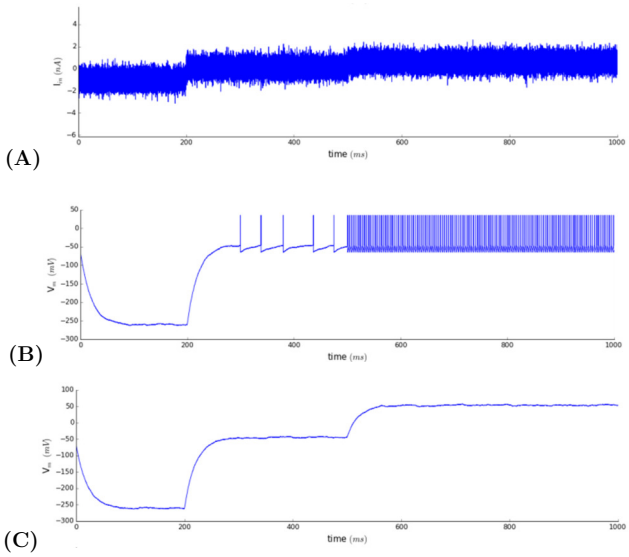

Figure 1.3. Leaky integrate-and-fire integration. A. Input noisy step current. **B.** Evoked membrane potential as a response to the step current in A. **C.** Same as B but with inactivation of the above-threshold reset mechanism.

Different step currents composed with noise (Fig. 1.3A) were used as inputs to a LIF neuron to study its reaction. For negative current steps, the membrane potential decreases down to a steady-state value whereas small positive currents cause repetitive firing. Larger inputs cause more vigorous and periodic firing (Fig. 1.3B). Fig. 1.3C reflects the same evolution but without action potentials (the reset mechanism was inactivated). As

expected, injecting a practically constant current into a neuronal cell causes the membrane potential to vary gradually with a time course governed by the membrane's passive properties.

The LIF is the simplest model that accounts for the effects of input current on output voltage. Mainly, one can see the firing rate increases accordingly with the input current above the threshold. The LIF model reproduces the basic firing properties of neurons.

1.3 The Hodgkin-Huxley model

Based on the analysis of the giant squid axon, the Hodgkin-Huxley model[17] (1952) is one of the first mathematical models which succeeded in reconstructing the generation of an action potential using biologically relevant parameters. It assumes that the neuron membrane has three types of independent channels: the leakage channels, the potassium channels and the sodium channels. Cycles of hyperpolarization or depolarization of the cell as a consequence of ion flows are responsible for the generation of action potentials.

1.3.1. HH variables and equations

Supposedly, all channels are composed of individual gates, following first order kinetics, that must be open simultaneously in order for a channel to be open. Activation gates open with depolarization whereas inactivation gates open upon hyperpolarization. Na^+ channels are composed by 3 fast activation *m*-gates and a slow inactivation *h*-gate, while K^+ channels are composed by 4 fast activation *n*-gates. Voltage-dependent variables *n, m* and *h* describe the probability of the gates to be open. As they all must be open at the same time, the overall probability of a channel to be open is the product of single probabilities, leading to voltage-dependent conductances of K^+ and Na^+ channels[41].

$$C_m \frac{dV_m}{dt} = I(t) - g_L(V_m - V_L) - \overline{g_K} n^4 (V_m - V_K) - \overline{g_{Na}} m^3 h (V_m - V_{Na}) \tag{1.5}$$

$\overline{g_K}$ and $\overline{g_{Na}}$ are the maximum membrane conductances to K^+ and Na^+ ions. The temporal evolution of *n, m* and *h* is given by the rate equation 1.6, where α_i and β_i correspond to the opening and closing rates respectively. Dependence of the opening and closing rates and values of the parameters are given in Section S2 of the Supplementary material.

$$\frac{di}{dt} = \alpha_i(V_m)\left(1-i\right) - \beta_i(V_m)i \quad , \quad i = \{n,m,h\} \tag{1.6}$$

1.3.2. Steady-state gate variables and timescales

At equilibrium and when no external current is applied, the inwards and outwards ion flows must compensate each other, leading to the equilibrium equations 1.7 and 1.8. The latter is obtained rearranging terms in equation 1.6. It is straightforward to appreciate the mechanisms for the generation of an action potential from the analysis of the dependence of the gate variables on the membrane potential (Fig. 1.4A, B).

$$\alpha_i(V_m)\left(1-i_{eq}\right) - \beta_i(V_m)i_{eq} = 0 \quad , \quad i = \{n,m,h\} \tag{1.7}$$

$$\tau_i(V_m) = \frac{1}{\alpha_i(V_m)+\beta_i(V_m)} \quad , \quad i = \{n,m,h\} \tag{1.8}$$

At resting potential, both types of channels are most probably shut. Upon depolarization, the *m*-gates rapidly open and the neuron's membrane conductance for Na^+ ions increases. When the activation threshold is reached, depolarization is actively driven by the cell up to +30 mV. Then, the opening of the *n*-gates at a relatively slower rate as well as the slowly shut *h*-gates favor the repolarization of the membrane potential. The relatively slow rate at which *n*-gates shut is responsible for the hyperpolarization of the potential under its resting value during the *relative refractory period*. Slow dynamics of the *h*-gates make Na^+ channels remain inactive during the *absolute refractory period* and cannot respond to depolarization.

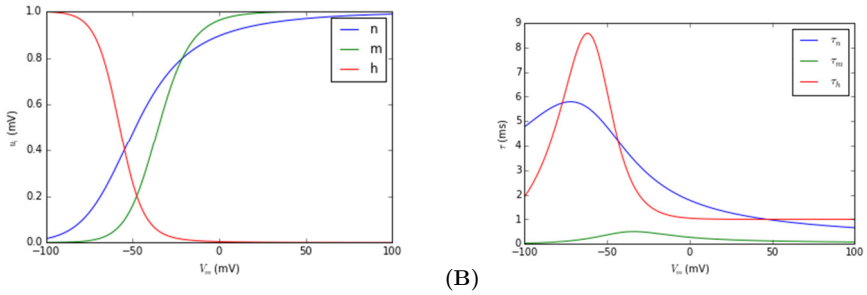

(A) (B)

Figure 1.4. Voltage dependency of the gating variables. A. Steady-state activation and inactivation variables as a function of the relative membrane potential. **B.** Time constants associated to each gate variable for the same range of membrane potentials as A.

1.3.3. Output membrane potentials to different input currents

A HH neuron was stimulated with a series of currents. First, the membrane responds to a negative input hyperpolarizing and the gate

variables shift towards the inactivation state. As expected, the afterwards shutting-down of the inputs drags the potential to its resting value. However, a postinhibitory rebound spike is fired immediately after the membrane's abrupt depolarization. This takes place whenever a long enough hyperpolarization is suddenly terminated[1]. Briefly, the net sodium conductance increases due to a fast increase of m and a slow variation of h upon depolarization. The input Na^+ current reaches the threshold and an action potential is fired. Then, increasingly positive currents show evidence of two phenomena. First, firing rate increases with the input. However, the fact that oscillations become faster damps the amplitude of the spikes. This is because gate variables do not have enough time to recover their original resting values for big inputs, which can eventually lead to extinguish the oscillations.

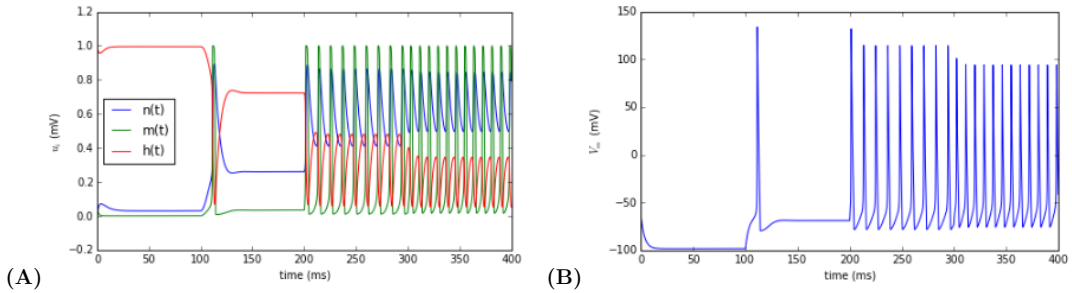

(A) (B)

Figure 1.5. Voltage response of a HH neuron upon steps of current. Successive values of the current, changing each 100 ms, where -10, 0, 20 and 50 nA/cm^2. **A**. Time-evolution of the three gate variables during stimulation. **B**. Voltage response of the cell membrane.

1.4 Conclusion

Spiking models combine passive and active properties of neurons, their complexity arising from the number and types of inputs taken into account. The leaky integrate-and-fire is simple but rather unrealistic, as it only models subthreshold activity. On the other hand, the Hodgkin-Huxley model is biologically very accurate but inefficient for computing large-population dynamics. Other versions of the LIF neuron, such as the adaptive exponential LIF[3,26], account for more complex synaptic adaptive dynamics[18] that will not be covered in this project.

Chapter 2

Experimental methods

Previous research of the Reyes group is based on experiments on active cortical slices[22,28,29] rather than *in vitro* grown cultures. Many advantages come from culture preparation for the analysis of network recurrent dynamics. The fact that the culture can be practically considered monolayer thus allowing precise localization of the neurons and the stimulus is one of them. This section focuses on the experimental methods used during the project. However, as the entire experimental set-up was put together by Dr. Jérémie Barral[2], only an introductory description of the instrumental devices and culture preparation will be provided here.

2.1 Introduction to culture preparation

Neuron cultures were made from dissociated cortical neurons taken from postnatal day P0-P1 mice cortex. Briefly, the mouse cortex is dissected in cold dissection solution (Ca^{2+} and Mg^{2+} Free Hank's balanced salt solution), the meninges (containing glial cells) removed and the remaining tissue enzymatically dissociated in papain (containing DNase). After enzymatic inactivation, tissue pieces are mechanically fragmented with a pipette and cells are plated on a glass coverslip inside a Petri dish filled with neurobasal medium. Cultures are let to grow in a humidified incubator (at 37ºC, 5% CO_2) for approximately 15 days, up to when the neuronal properties and network connectivity are supposed to have reached a steady-state value[28,29] and electrophysiological recordings are reliable.

Some of the cultures are infected virally with Channel rhodopsin-2 (ChR2) so as to use optogenetic techniques to photostimulate the network. The cultures in question are injected with 1µl of ChR2 at three days *in vitro*. ChR2 can be expressed in both E and I neurons. The expression of ChR2 is mature enough when the cultures have grown so as to allow consistent photostimulation (see Section 2.4).

2.2 Visualization of neurons in culture

Neurons in culture are visualized through an Olympus water-immersion objective in ACSF (x10 magnification). Cells are viewed, counted and patched under infrared differential interference contrast videomicroscopy (Fig. 2.1; IR-DIC). Neurons expressing ChR2 are viewed using fluorescence microscopy (Fig. 2.3B).

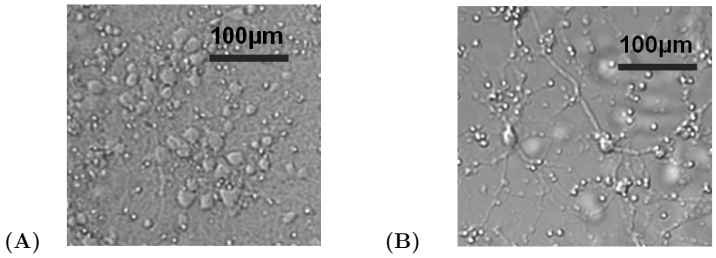

Figure 2.1. Visualization of neurons in culture with IR-DIC microscopy. **A.** Neurons in a dense culture. **B**. Neurons in a sparse culture. It is easy to distinguish healthy neurons (big and with dark edges) with dead ones (small and shiny or big and with diffuse edges).

The interelectrode distance, which is an important piece of data for our analysis, was measured with image treatment software ImageJ. All pictures were calibrated with reference to a known 1 mm object.

3.3 Patch clamp techniques

Recordings from neurons in culture via a patch electrode are made at room temperature in oxygenated artificial cerebrospinal fluid (ACSF). The recording electrode is put into a hollow borosilicate micropipette filled with an electrolyte similar to the intracellular medium. The pipette's resistance varies from 6 to 12 MΩ and can be measured when a step voltage is applied in voltage clamp mode. Upon approaching the cell, a negative offset sets the electrode voltage near the cell's resting potential. Immediately after touching the cell, a slight increase in the resistance measured by the electrode is noticeable, as a combined effect of the membrane channels. Applied negative pressure sucks a small *patch* of the membrane into the pipette. The membrane can be ruptured by brief pulses of suction once the seal reaches a value around 1 GΩ (whole-cell, Fig. 2.2C) or maintained attached to the pipette if it remains lower (cell-attached, Fig. 2.2B). Finally, the mode is switched to current clamp, allowing to measure variations in the membrane potential of the neuron.

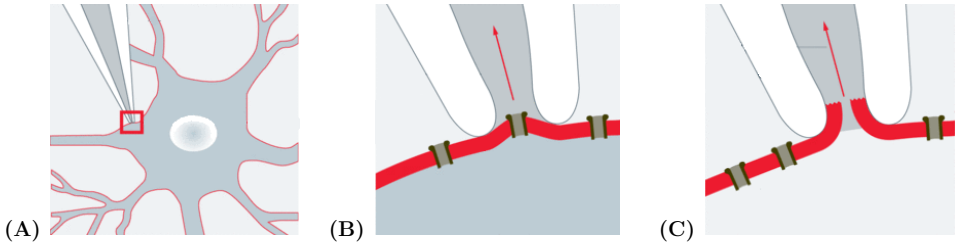

Figure 2.2. Schematics of the configuration for patch clamp. A. Location of the electrode on the neuron to patch. **B.** Cell-attached (CA) current clamp and **C.** Whole-cell (WC) current clamp techniques[40].

The rupture of the membrane for whole-cell recordings establishes a direct electrical connection with the intracellular medium[30,34]. Consequently, the current measured by the micropipette is due to all of the cell's ion channels. The effect of the series resistance of the pipette is negligible for cells as small as the ones in culture, for they have high membrane resistances.

Another recording mode, the so-called cell-attached recordings, are similar to whole-cell except that the membrane is not ruptured. This extracellular recording allows detection of only large action potentials. Being so, ion flows between the interior of the cell and the pipette's solution can only occur through the ion channels that lie on the patch of membrane.

2.4 Set-up for optogenetic stimulation

Some of the cells in culture express Channel rhodopsin-2 (ChR2), a transmembrane protein that is sensible to blue light, its maximum peak of absorption being around 480 nm. The absorption of a photon induces two consecutive conformational changes of the protein, opening the ion channel and allowing the flow of ions. This makes cellular depolarization straightforward and very useful for photostimulation[2].

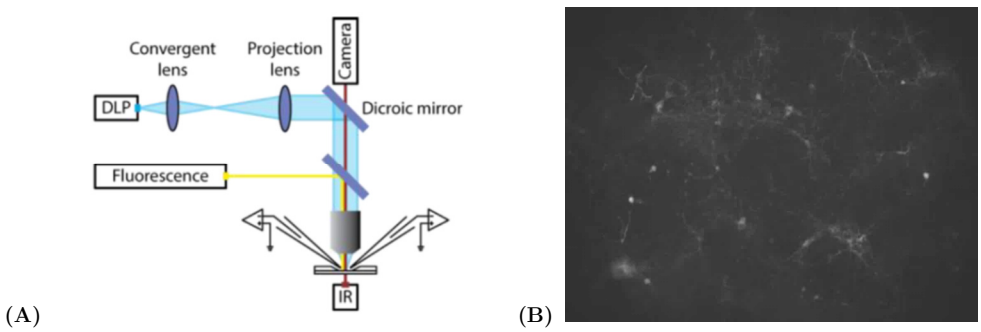

Figure 2.3. Visualization of fluorescent cells expressing ChR2. A. Set-up for stimulation and visualization of fluorescent cells. **B.** Example of ChR2-expressing culture visualized with fluorescence microscopy.

Our cultures can be stimulated using optogenetic techniques, a photostimulation method that involves the use of light to control cells that have been genetically modified to express light-sensitive ChR2 ion channels. A Digital Light Processing projector (DLP; see Fig. 2.3A) is used to deliver spatiotemporally accurate light pulses centered at 460 nm. When a small diameter light beam is presented to the cell, action potentials are generated. We stimulate cells within a region of interest (named ROI, dimensioned 1.73mm × 0.96mm) with Poisson train pulses at a rate of 5Hz and 0% temporal correlation. Recordings are registered from neurons that do not express ChR2, so as to avoid any correlation coming from the input. However, we hold no knowledge whether the stimulated neurons are excitatory or inhibitory.

2.5 Conclusion

Our experimental approach consists on performing electrophysiological recordings of membrane potentials of live cortical neurons in *in vitro* cultures during spontaneous activity and optogenetic stimulation via whole-cell and cell-attached patch clamp measurements. The membrane potentials recorded with patch clamp techniques have a temporal resolution in the range of the ms. Also, as we mentioned before, *in vitro* cultures of neurons can be practically considered monolayer and glia free, allowing to count cells with an easy tactic. Studying the cells in cultures will allow us to, first, carry on a thorough characterization of the neurons and their connectivity. The detailed analysis of electrophysiological data will, on the other hand, provide valuable information about network activity and the mechanisms at the origin of population bursts.

Chapter 3
Characterization of networks' properties

A preliminary analysis of the neurons in culture permits the documentation of some of the network's properties. Although the neurons' intrinsic properties such as their membrane resistance or time constant have been widely documented in other preparations[2,22,28,29,31], we repeat these measurements in cultures for comparison and for getting useful parameters for the simulations. The parameters needed for the model include, besides from the intrinsic properties, the density, the patterns of connections and the synaptic properties.

3.1 Culture density and spatial structure

Cultures of neurons with different density of cells/mm^2 were prepared. Density can be controlled at the early stage of culture preparation when the cells in suspension have to be diluted into neurobasal medium. It was calculated for each culture of neurons (Fig. 3.1) using Adobe Photoshop by counting single neurons on different spots of the culture. Although neurons are clearly heterogeneously distributed in the cultures (see Fig. 3.2B), bars in Fig. 3.1 represent the mean and standard deviation of a number of densities calculated for each culture.

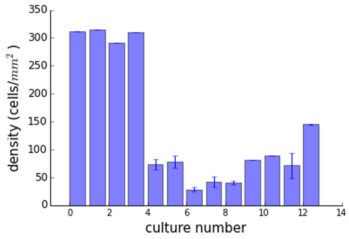

Figure 3.1. Density of the cultures of neurons. Bar chart with error bars documenting the calculated network densities for a total of 12 cultures. For some cultures, density was calculated based on a single picture, thus the variance was considered null.

Then, a superposed layer was created so as to mark the center of each cell and obtain the geometrical distribution of the nodes (the neurons) in the network. One can notice that the spatial distribution of the cells ranges from random (Fig. 3.2A, C) to increasingly grouped at higher culture density (Fig.

3.2B, 3.2D). Although Fig. 3.2B and D are only two examples, the presence of these groups of neurons was a generalized characteristic of dense cultures. We will call these groups "clusters" of neurons. There is, however, a large fraction of cells that do not belong to any cluster even when the density is high. Simulations in Chapter 5 will try to reproduce this architecture.

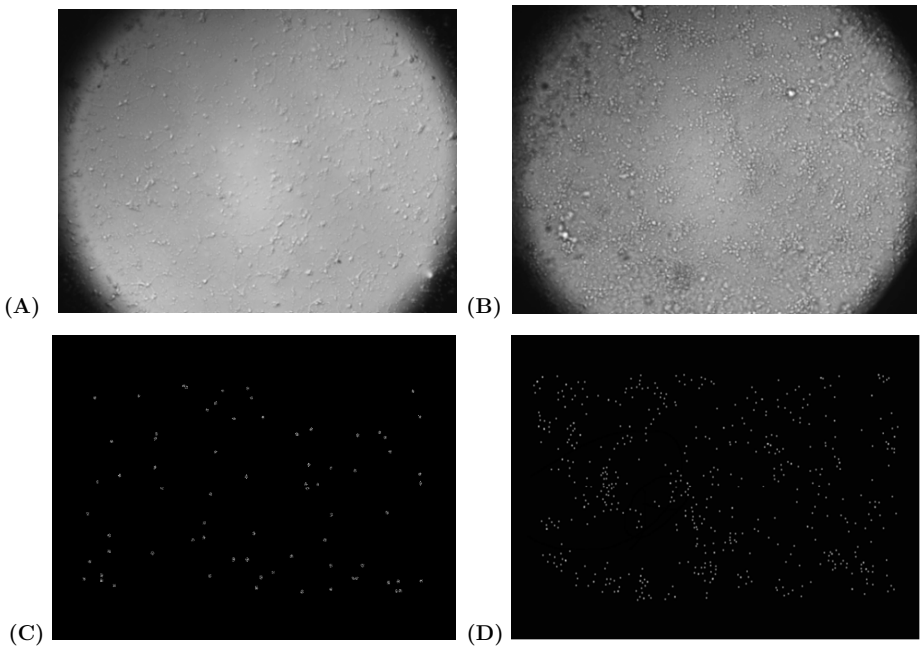

Figure 3.2. Visualization and spatial distribution of the neurons in culture. A. Very sparse culture (70 cells/mm^2) and **B**. very dense culture (300 cells/mm^2) observed via infrared microscopy. **C.** Geometry of a sparse culture of neurons and **D**. a highly dense culture of neurons.

Theoretical studies based on clustered networks of E and I neurons suggest they exhibit transitions between low and high activity states[23] .Thus, heterogeneity in network structure could account for neural variability in both spontaneous and stimulated regimes. As non-clustered networks would only lead to asynchronous dynamics, clustering could be a mechanism for the generation of population bursts.

3.2 Synaptic connectivity

It is the recurrence of the connections in the network created after culture maturation that allows for internal dynamic states of spontaneous activity. To determine whether two neurons are connected, we stimulate one neuron with steps of current (Fig. 3.3A) while measuring the voltage response of other cells (Fig. 3.3B). The result is very straightforward, as an evoked unitary postsynaptic potential will appear only if the neurons are connected

to each other. We examined the connectivity profile of a number of cultures and extracted their synaptic properties. Finally, we classified as many patched neurons as possible as being excitatory or inhibitory. The color of the voltage and current traces (see Fig. 3.3) simply refer to the electrode used to record them (black, red, blue or green).

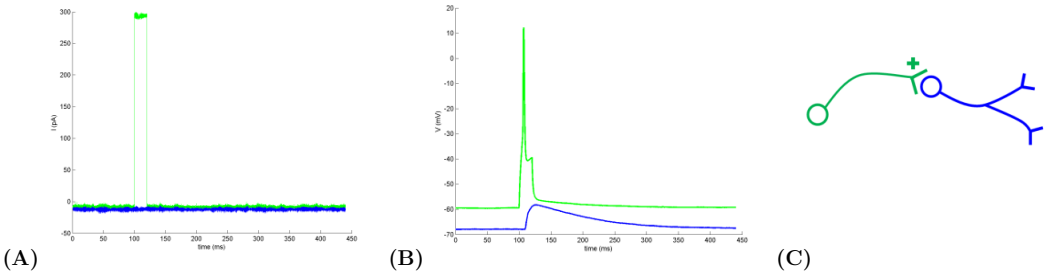

Figure 3.3. Successful test of neuronal connectivity. A. A step current is injected to the green neuron. **B**. Induced spike in the green neuron due to the input current and evoked EPSP in the blue neuron. **C**. Schematics of the situation in B: the blue neuron is connected to the presynaptic excitatory green neuron. The sketch assumes the connection is monosynaptic and other neurons in the network are not depicted.

A connectivity profile from all the recorded cultures was computed (Fig. 3.4). As there is a clear preference for neurons to be connected if they are nearby each other, this result supports previous findings stating connection probability decreases with the distance[2,22]. Also, this result proves that neurons in cluster are probably connected to each other

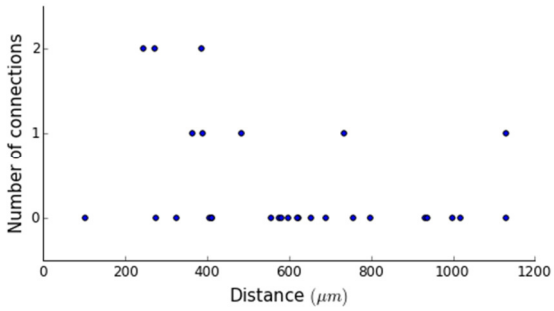

Figure 3.4. Connectivity profile within all cultures of neurons. The number of connections between a pair of neurons (with known interneuron distance) can either be 0, 1 or 2.

3.2.2. Synaptic properties

a) Testing the neurons' functionality

It is also very useful to determine the identity of the patched neurons. A priori, neurons cannot be classified as I or E on the basis of action potential waveform alone[10]. However, neurons can be classified based on whether an EPSP (see Fig. 3.6A) or an IPSP (see Fig. 3.6B) is induced in the

neighboring neuron. Using this criterion, a total of 3 inhibitory and 7 excitatory neurons were classified, which is close to the approximate 25% ratio of the number of inhibitory over excitatory cells in cortical networks[2,27].

b) Amplitude and delay

For neurons that are separated by long distances, it is possible that the evoked PSPs were mediated via intermediate neurons (polysynaptic as opposed to monosynaptic). We therefore measured the time delay between the start of the stimulus and the response PSP. Although the amplitude of both EPSPs and IPSPs is decreased slightly at long distances (Fig. 3.5A), our limited number of data are still inconclusive. The same applies for the time delay (Fig. 3.5B). IPSPs seem indeed to appear later when the distance between stimulated and measured neurons grows, but nothing can be extracted for the excitatory neurons.

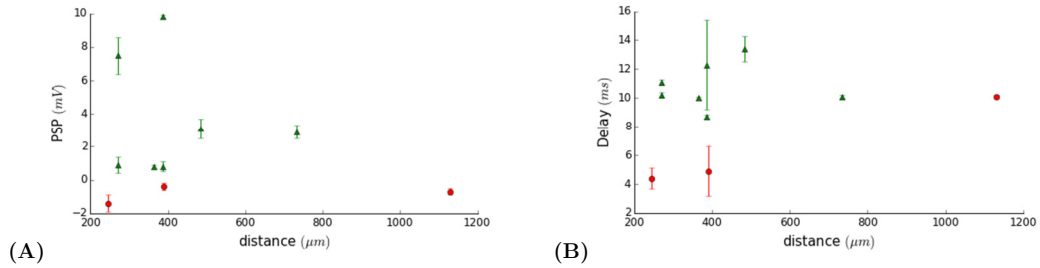

Figure 3.5. Synaptic strength and time delay. A. Amplitude of the evoked PSPs as a function of interneuron distance. **B.** Time delay between the start of the stimulation and the initiation of the evoked PSP. Data was recorded from 3 inhibitory neurons and 7 excitatory neurons.

c) Synaptic depression

Finally, the connectivity test reveals the effects of short-term synaptic depression, which is a type of synaptic adaptation. Both E and I synapses lose their efficiency due to repetitive firing activity but it recovers after a sufficiently long delay (Fig. 3.6). Three pulses were delivered in rapid succession and the ratios of the amplitudes of the $1^{st}/2^{nd}$ and $1^{st}/3^{rd}$ PSPs were documented. On average, EPSPs decreased a 22% from $1^{st}/2^{nd}$ and a 42% from $1^{st}/3^{rd}$ while IPSPs were reduced by a 43% and a 41%. Thus, adaptation is more significant for inhibition than for excitation.

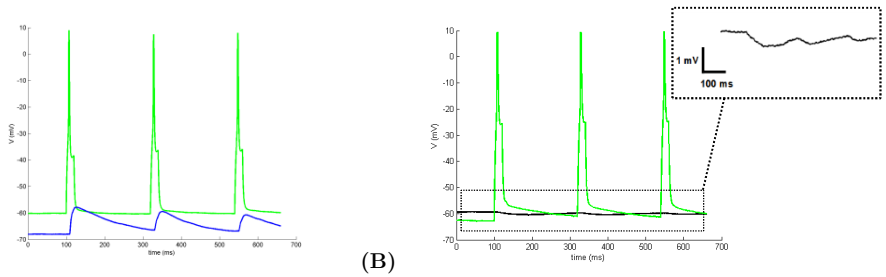

(A) (B)

Figure 3.6. Evidence of synaptic excitatory and inhibitory depression. A. The green neuron's excitatory synaptic strength is depressing after firing the first action potential. The amplitude of the evoked EPSPs in the blue neuron becomes smaller. **B.** Same than for A but in the inhibitory case scenario. The evoked IPSPs in the dotted box region were magnified so as to appreciate the scale of inhibitory depression.

Simulations in Chapter 5 account for this phenomenon, as it is thought to play an important role in damping excitation and thus limiting the duration of population bursts. Differences in the adaptation of EPSPs and IPSPs may be a mechanism of E/I imbalance.

3.3 The V/I test

The V/I test is conducted in current clamp mode once the cellular membrane has been ruptured. It consists on stimulating a neuron with increasing steps of current (upper-left panel, Fig. 3.7) and measuring the voltage response (upper-right panel, Fig. 3.7). Not only this is a very effective way to check whether the patch holds, but it is also a reliable technique to calculate cell parameters such as the membrane resistance or the time constant. Data fittings were performed with Matlab (`polyfit` and `fit` toolboxes).

3.3.1. The GUI interphase

In order to make the data analysis of the V/I tests interactive and more effective, I developed a GUI Matlab graphic interphase. The program allows the user browsing a file containing the data, plotting, saving and treating it to withdraw cell parameters.

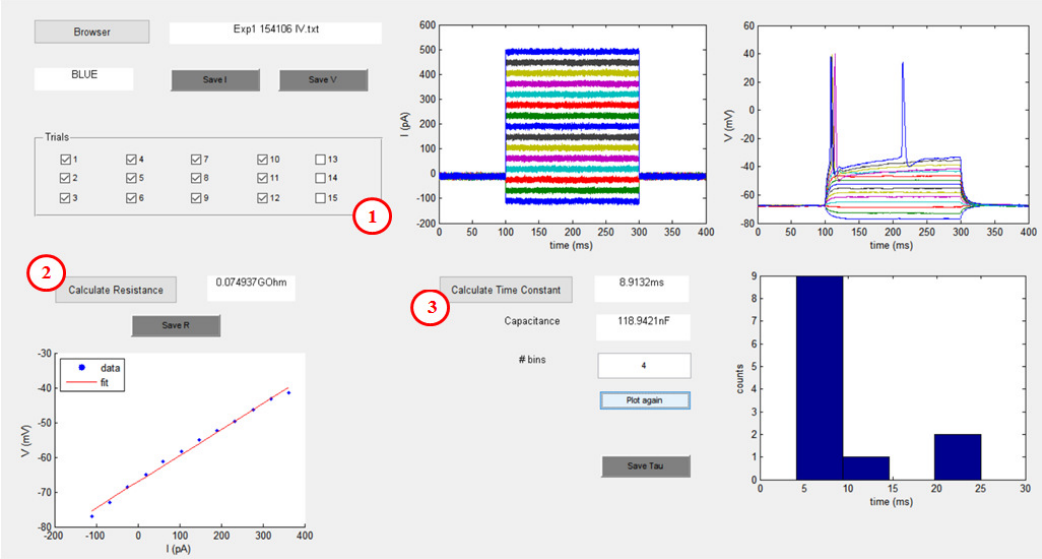

Figure 3.7. Graphic GUI interphase of the I/V test. All panels include options for plotting and saving the data. Panel (1) allows the user to select the trials he wants to calculate intrinsic parametrs, the lowest current value corresponding to trial 1. Calculations become more accurate when spiking signals are rejected. Panel (2) calculates the membrane resistance with a linear regression. Panel (3) calculates the membrane time constant τ and capacitance, appart from allowing the user to chose the number of bins in the τ-histogram.

3.3.2. Calculation of intrinsic membrane properties

The cell membrane intrinsic parameters can be withdrawn from averaged results over tests.

In most of the tests, the voltage response of the cell reaches equilibrium after a lapse of time related to the membrane time constant and which value depends on the injected current. One can easily notice there is a linear dependence between the steady-state voltage and the input current (Fig. 3.7, bottom-left panel), the slope being the membrane resistance. In order to obtain an estimate of the time constant, an exponential fit of the selected tests was performed assuming a saturating exponential growth. Gaussian fits of the obtained resistance and time constant histograms (Fig. 3.8) gave mean parameters R_m=*196±64 MΩ* and τ_m=*22±10 ms*.

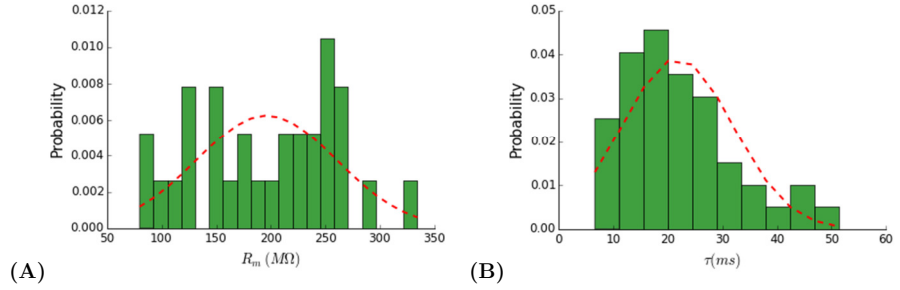

Figure 3.8. Intrinsic cell parameters. Histograms and Gaussian fittings of membrane resistances (A) and time constants (B) for 44 patched cells.

3.3.3. Comparison to the HH model

The voltage response upon increasingly positive currents creates firing patterns that strongly remind of those obtained with the HH model (Fig. 3.9B). The neuron starts firing once the threshold is reached, and oscillations become faster and drastically damped for high values of the current.

Note from these and the previous analyses that the voltage response of a single cell to current steps does not initiate the propagation of population bursts within the network, indicating it has to be a "population-wide" event.

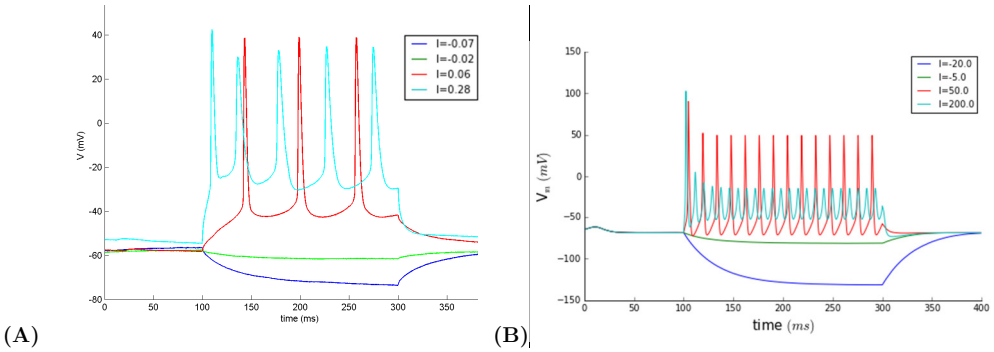

(A) (B)

Figure 3.9. Voltage response to successive step currents. A. Experimental results for a cell with 450 MΩ membrane resistance for input currents in nA. **B.** Results from the HH model for input currents in nA/cm^2 and a leakage conductance of 0.3 µS/cm^2.

3.4 Conclusion

Overall, results in this chapter are comparable to previous research. The spatial distribution of E and I neurons in the culture becomes increasingly clustered at higher network density. As for synaptic depression, it appears inhibition adapts more than excitation upon successive firing, which could be a mechanism underlying E-I imbalance. Neuron intrinsic parameters and E/I proportion seem similar to those measured previously in cortical slices[2,22,28,29]. However, we did not specify excitatory and inhibitory parameters due to the poor information we had on cells' identities. Finally, the fact that the stimulus of a single cell did not evoke the generation of a population-wide burst indicates these events must be due to network activity. This will be exhaustively studied in the next chapter.

Chapter 4

Characterization of population bursts during spontaneous and stimulated activity

Neurons exhibit spontaneous firing that is often noisy. Typically, single action potentials occur infrequently and to a first approximation follow Poisson-like statistics[14]. However, spontaneous bursts are observed in some of the whole-cell and cell-attached recordings. This chapter focuses on an exhaustive analysis of electrophysiological recordings in neural cultures. After enumerating the main characteristics of spontaneous population bursts that make them stand out from asynchronous dynamics, we will try to elucidate some of the mechanisms responsible for their emergence. We hypothesize that the bursts result from a breaking of the excitatory-inhibitory balance in the network and from there investigate which mechanisms could be at the origin of the rupture.

To analyze the data from electrophysiological recordings, I developed a GUI Matlab graphic interphase. The program inputs the voltage trace automatically and allows to calculate pairwise correlations of membrane potentials.

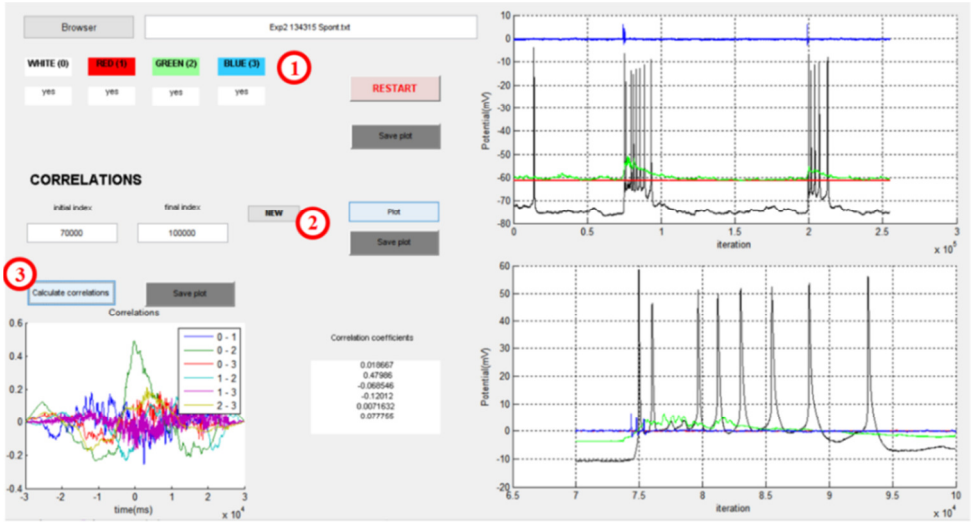

Figure 4.1. GUI graphic interphase for the analysis of electrophysiological recordings. Panel (1) allows to read, plot and save the data while indicating the measuring electrodes. Panel (2) allows to choose an initial and final iteration to zoom the data. Panel (3) calculates pairwise cross-correlations and correlation coefficients of the zoomed membrane potentials.

4.1 Differences between the asynchronous and bursting states

4.1.1. Bursts are "population-wide" events

During a burst, multiple action potentials often occur in rapid succession over approximately 1s (Fig. 4.2). Shorter and subthreshold bursts were also recorded, so an added criterion for classifying a neural event as a population burst is that all of the recorded neurons undergo a protuberant collective burst oscillation[24,36]. This excludes bursts generated spuriously in single cells due to, for example, a sudden change in the dynamics of its ion channels. For instance, in Fig. 4.2, two single action potentials (black stars) occur in the black neuron that were not exhibited in the others. In contrast, the long duration burst (red star) was present in all neurons.

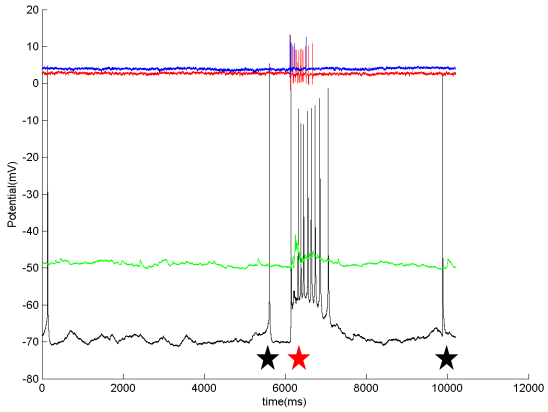

Figure 4.2. Spontaneous asynchronous and bursting activities. The red and blue electrodes were cell-attached, the green and black ones were whole-cell and at rest. Spikes are detected on the blue and red electrodes when a population burst occurs. Black and green electrodes also record subthreshold activity during this collective neural event. The red star indicates the beginning of the population burst and the black stars single action potentials.

4.1.2. Increased pairwise correlations

A succession of alternate asynchronous (Fig. 4.3B) and bursting states (Fig. 4.3C) is observed in most of the intracellular recordings. Most of the time, the cells are silent with small fluctuations in the membrane potentials (dashed box). Occasionally, population bursts occur (dotted box). To quantify the level of synchrony, we performed pairwise correlations of the membrane potentials.

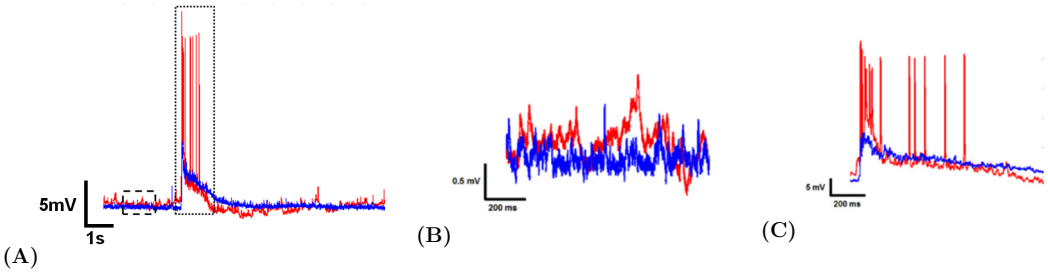

(A) (B) (C)

Figure 4.3. Dual behavior of membrane potentials. A. Recording over 10s of the membrane potential from two patched cells separated by 1.35 mm. **B**. Amplified plot of the dashed boxed region in A. **C**. Amplified plot of the dotted box region in A.

As expected, the voltage fluctuations in cells are weakly correlated during the asynchronous state (Fig. 4.4A, blue) but become correlated during the collective protuberant synchronous oscillations (Fig. 4.4A, green). Whether this is a general feature of bursts was confirmed by computing the correlation coefficients of the membrane potentials of pairs of neurons (recorded in whole-cell patch clamp) in two of the cultures (Fig. 4.4B). Pearson coefficients were always positive and noticeably higher when bursts occurred.

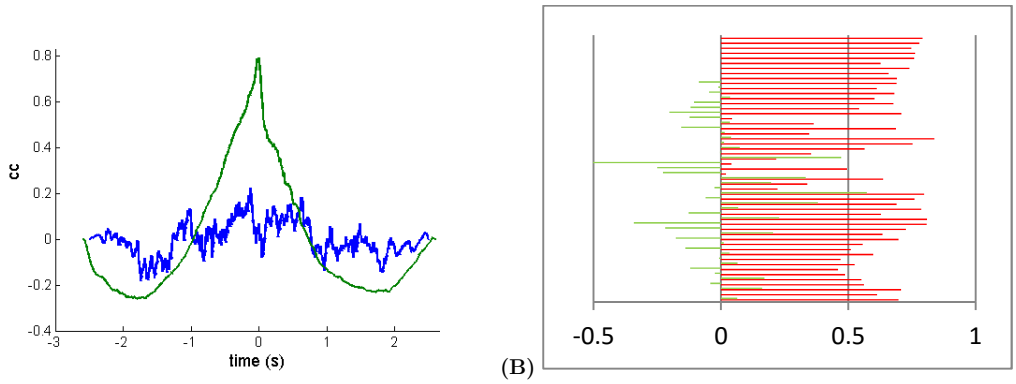

(A) (B)

Figure 4.4. Pairwise correlations during bursting and asynchronous dynamics. A. Cross-correlation of the two signals in Fig 4.3B (blue) and C (green). **B.** Pairwise correlation (Pearson) coefficients of membrane potentials where at least a population-burst was recorded (red bars) and from data where no bursts appeared (green bars).

4.1.3. Isolated postsynaptic potentials during bursts

When the membrane potential is near its resting value, the neuron receives a combination of E and I inputs. Estimating the relative amplitude and timing of E and I contributions is crucial for elucidating the underlying E-I dynamics[27].

The following technique allows to separate either the I or E contributions to the total synaptic input. E may be isolated from I by injecting steady

current through the electrode and hyperpolarizing the cell so that V in equation 1.2 is equal to V_i*(=-80mV)* making I_i*=0* (Fig. 4.5B). I may be isolated from E similarly by making $V=V_e$ (Fig. 4.5A). Thus, isolated IPSPs or EPSPs respectively will be recorded. In practical terms, membrane potentials will (ideally) exhibit only negative or only positive polarities and will be biased by 0 mV and -80 mV respectively.

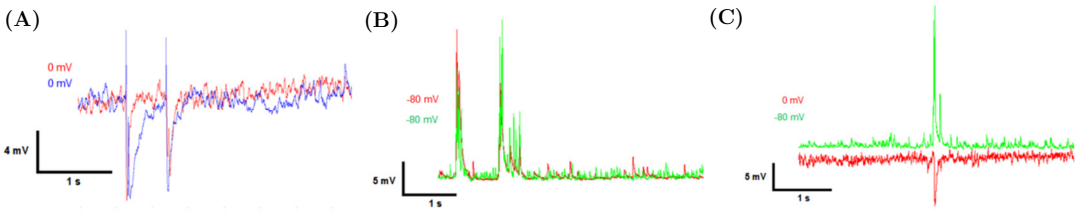

Figure 4.5. Membrane potentials from a pair of neurons during population bursts. A. Both electrodes held at the reversal potential of excitation. Isolated IPSPs. Pearson correlation coefficient *r=0.350*. **B.** Both electrodes held at the reversal potential of inhibition. Isolated EPSPs. *r=0.714* . **C**. Hyperpolarized green electrode and depolarized red electrode. Isolated EPSPs and IPSPs respectively. *r=-0.363*.

Figures 4.5A-C make evident all cells receive large amounts of correlated E and I inputs during population bursts that arise from network activity. In A, two simultaneously recorded cells show co-variation of large I and in B, two cells show co-variation in E. The classical theory of balanced networks predicts asynchronous potentials across pairs of neurons due to a close tracking of I upon E[2,31,39]. During tracking, the E tends to be counterbalanced by I in time. A closer look on asynchronous traces shows there is indeed a mild tracking (Fig. 4.6A, black stars) that is confirmed by a peak near the origin in their pairwise correlation (Fig. 4.6B).

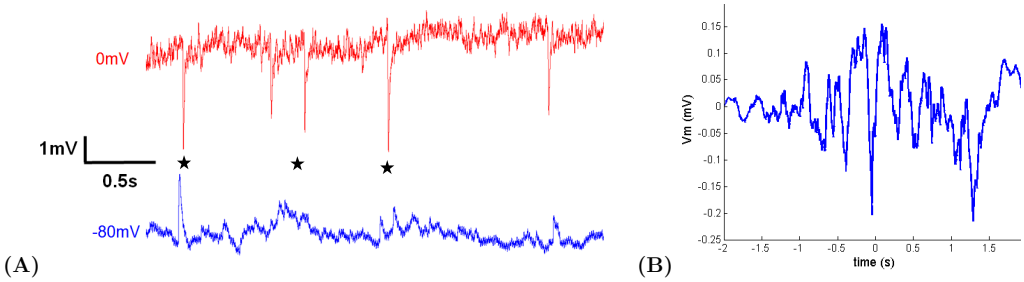

Figure 4.6. Asynchronous dynamics in balanced state. **A**. Hyperpolarized (blue) and depolarized (red) membrane potentials during asynchronous activity. **B**. Cross-correlation of the pair of neurons in A. The Pearson coefficient is *r=-0.008*.

Isolated PSPs also allow to quantify the relative amplitude and timing of E and I during both activity regimes. Taking traces in Fig. 4.5C as an example and amplifying them we see the ratio of E/I amplitudes is around

0.83 during asynchronous behavior (Fig. 4.7A) and 1.88 during the burst (Fig. 4.7B). As for the time lag, the I burst starts approximately 2 ms after the E one. A deeper and numerical analysis should be done to get reliable values of these two parameters. However, this early calculation proves E and I are roughly balanced in cultures except during infrequent bursts when E massively overwhelms I.

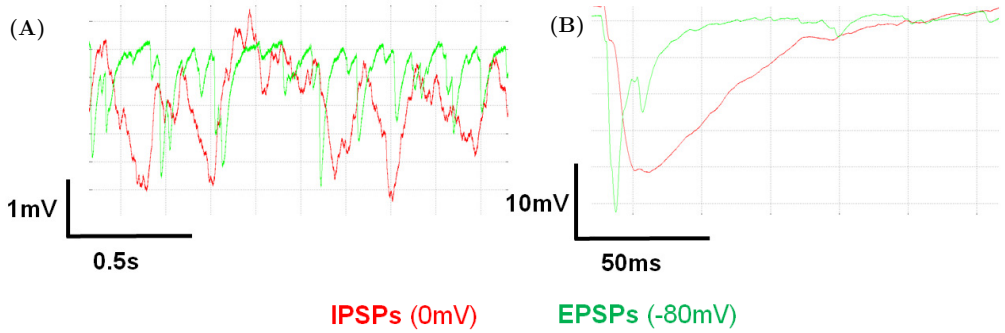

Figure 4.7. Amplitude and timing of E and I. Recordings from depolarized (red) and hyperpolarized (green) neurons. The green trace was flipped and put at the same level as the red one so as to compare them properly. **A**. Potentials during asynchronous regime. The mean amplitudes are 2.3mV for E and 2.8mV for I. The lag was not quantified. **B**. Potentials during a burst. The mean amplitudes are 15.4mV for E and 8.2mV for I. The lag was -1.9 ms, I tracking E.

We corroborated bursts that occasionally appear in electrophysiological recordings are population-wide events of synchronous activity. Whereas a balance between E and I is maintained during most of the dynamics, population bursts are characterized by a temporary rupture of this equilibrium that is obvious from the ratios of E/I amplitudes.

4.2 Burst frequency

Previous measures performed by the Reyes lab observed spontaneous bursts occurring at a mean rate of 0.1-0.5 Hz. This result was also supported by another research group that performed experiments on slices of prefrontal and occipital cortex of ferrets[36]. One of our predictions was that the burst frequency should depend on the number of cells in the network. Should the network be too sparse, then the recurrent activity would be too small to originate any burst and none should be recorded. On the other hand, the denser the network becomes, the more number of connections there are and recurrent activity becomes more important.

Based on a series of recordings of bursting activity, we were able to gather some data to appreciate an apparent dependence of their mean rate on

the network's density (Fig. 4.8). As expected, there are no or very few population bursts for densities below 80 cells/mm^2 approximately. The frequency increases rapidly afterwards. Then, the dependence becomes more uncertain, as it remains above 0 but it is apparently lower than for intermediate densities. A study on neural avalanches[4], which are similar to bursts, predicts a complete extinction of the avalanches for sufficiently large networks.

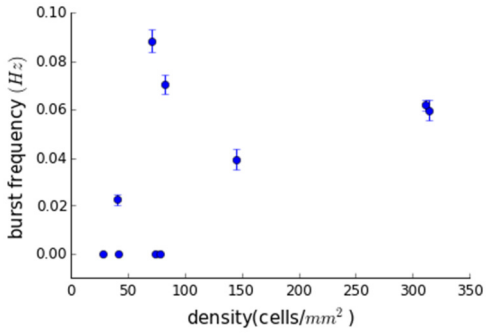

Figure 4.8. Bursting frequency as a function of network density. Points with null variance are those for which no burst was recording (rate=0Hz).

4.3 Burst duration

Next, we examined the dependence of the burst duration on the density. For this analysis, we only took into account data where both the beginning and the end of the burst were recorded. Fig. 4.9 shows two example recordings that were discarded. As this happened mostly for dense cultures, the computed results for high densities (Fig. 4.10) may be lower than the real value because of the strict discard criterion. Also, we considered a burst any salient collective oscillation, despite the number of spikes or its duration.

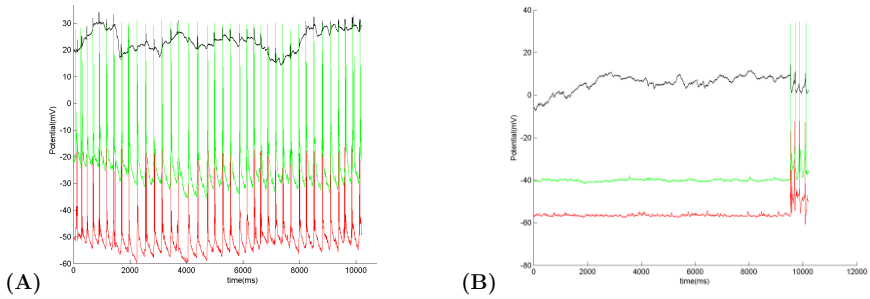

Figure 4.9. Example of rejected recordings. A. The burst is so long that it lasts the whole recording. **B**. The beginning of the burst is on record but its termination is not.

Unlike for the frequency, the burst duration appears to be clearly dependent on the network density, increasing linearly for the lowest densities in Fig. 4.10. The duration of the bursts seems to saturate for high frequencies

at roughly 2s. Although we cannot explain this apparent saturation at this point, it could be due to synaptic excitatory depression damping EPSPs and terminating the burst. Comparing these results with Fig. 4.8, cultures that burst more frequently (with a density between 80 and 150 cells/mm^2 approximately) exhibit shorter bursts than denser cultures.

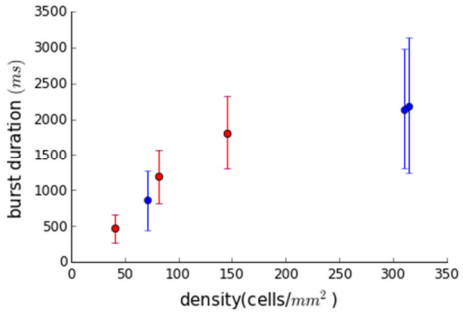

Figure 4.10. Burst duration as a function of the network's density. To compute the burst duration as a function of network density, we calculated graphically the duration of all the bursts in a set of data, fit the obtained distribution with a Gaussian variable and plotted the mean and variance for each known density. Thus, each point summarizes the information from recordings on a single culture of neurons. In three cultures with low density (red dots) an extremely long burst was recorded. The latter was discarded to fit the data, as the variance reached unrealistic values.

We have proved bursts are population-wide events which frequency and duration tightly depend on the network density. On average, they last about 1s and occur at mean frequencies less than 0.1Hz for our cultures. Our next step is to investigate whether population bursts are generated randomly throughout the network or at specific locations.

4.4 Burst origin

One of the many possible mechanisms causing the imbalance between E and I and generating population bursts is an overwhelmingly excitatory input generated locally and propagated through the network.

A first evidence of the wave-like propagation of the bursts is given by calcium imaging techniques. Briefly, the cells are from transgenic mice that express a calcium channel indicator. When an action potential occurs, it opens up calcium channels in the cells, which in turn cause the cells to fluoresce because of the indicator[12]. Labeled neurons allow for real-time fluorescence visualization of the network activity. While lacking of temporal resolution due to the slow timescale of calcium (around 100ms), this method allows to make a rough prediction of where the burst starts. For example, in

Fig. 4.11, there are neurons in the upper-right hand corner (circled in red) that are initially silent (A) but become active later (B).

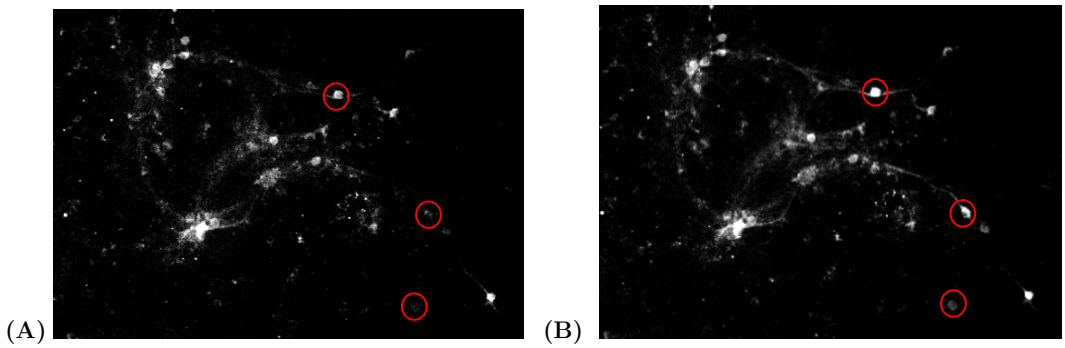

Figure 4.11. Fluorescence microscopy of calcium imaging. A and **B** are two consecutive photograms of a calcium imaging movie. Some neurons (red circles) are silent in A but active in B, which indicates the burst is propagating in the right direction.

To further support this theory, we inspected the order at which patched neurons started to burst. With electrophysiological recordings, we have temporal resolution in the ms range. Some criteria must be clarified before going into the detail of the results. First, only whole-cell recordings were analyzed, as cell-attached measurements do not reveal subthreshold activity. Secondly, the order in which the neurons started to burst was determined graphically. Finally, we always patched from 2 to 4 neurons relatively close to each other. Configurations in Fig. 4.12 refer to possible ordered combinations between neurons (for example *red-green-blue-black*) representing the chronological sequence in which they start to burst.

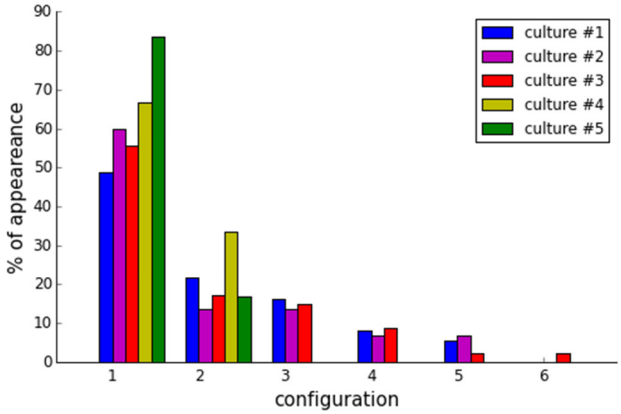

Figure 4.12. Documentation of the burst order. Each color represents a culture. The number of possible combinations between cells goes from 2 to 6 depending on the number of patched neurons. Bins in the bar chart represent the 6 configurations, ranked from the more frequent (1) to the less likely to appear (6) for each culture.

Indeed, results suggest that burst tend to originate in a particulate region of the network as a particular sequence tends to occur more often than

others. Although the number of trials was low to run conclusive statistics, there is a drop of more than a 20% in the likelihood of the second configuration with respect to the first in all of the cultures. The propagation seems to become more random from there, as the second and third bins are more similar to each other.

The hypothesis of the existence of a specific spatial origin of the population bursts is supported by this analysis. For some unknown reason, the neurons in this "hotspot" are more prone to burst. Once the burst occurs, it spreads to other parts of the network. One goal of future research is to determine what makes the neurons in the hotspot different from the others. A spatial heterogeneity of synaptic properties in the network could lead to regions with excessive number of excitatory cells or synapses, with slower inhibition or with stronger short-term synaptic depression of inhibitory cells.

This confinement of unusually excessive excitatory activity is also known to be the cause for some types of seizures, concretely partial seizures that affect relatively isolated regions of the brain[6]. There currently exists a surgical treatment to epilepsy consisting on removing the area of the brain producing seizures.

4.5 Evoked activity during optogenetic stimulation

Based on the above, our hypothesis is that there is a "hotspot" that generates excessive excitatory inputs to the other neurons, causing them to burst. One question is whether driving the neurons outside the hotspot can also cause population bursts. If not, then this supports the notion that there is something special about the neurons in that region.

We want to study the patterns that arise in simultaneously recorded cells that do not express ChR2 when ChR2-expressing neurons are stimulated with repetitive uncorrelated pulse trains of light. Inputs can be treated as background synaptic noise due to their small correlation. All stimulated cells lie within a small region of interest (named ROI). Thus, optogenetic stimulation could mimic the effect of excitatory activity being generated at the location where the burst originates. Where we to illuminate the right region, we would expect to record population bursts occurring simultaneously in all the cells. Membrane potentials where recorded from two depolarized and hyperpolarized in whole-cell configuration and from a third one cell-attached (Fig. 4.13).

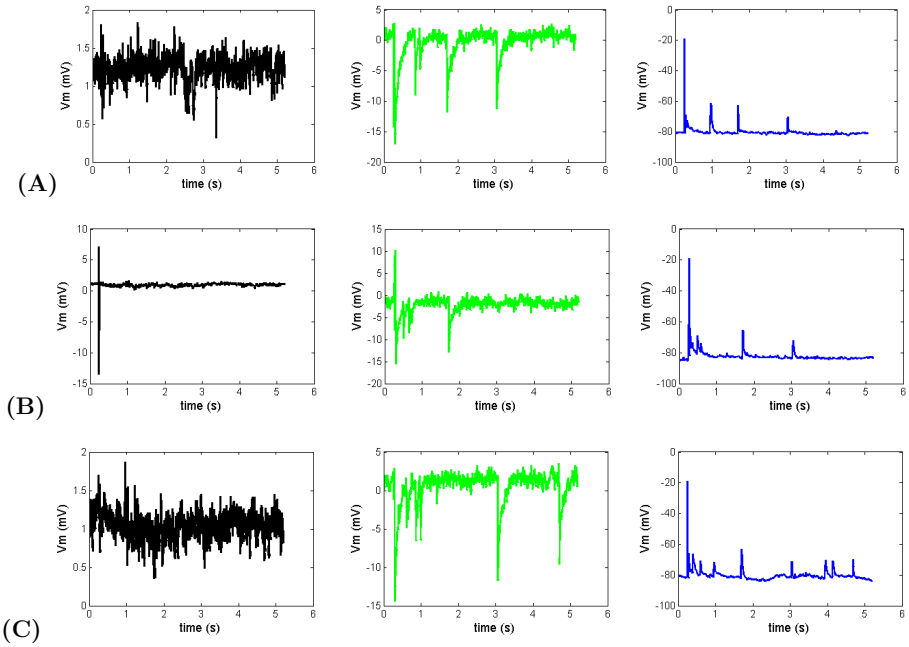

Figure 4.13. Patterns of evoked activity. A, B, and **C** represent the voltage traces from three simultaneously recorded neurons (black, green and blue) during three trials of the same input pattern. The black neuron is cell-attached, the green neuron is whole-cell and depolarized to 0mV and the blue neuron is also whole-cell and hyperpolarized to -80mV.

First of all, observing action potentials in neurons that are not stimulated is a proof of the recurrent activity of the network. Also, recorded traces varied from trial-to-trial (i.e. population-bursts were not generated), but more importantly, the responses of the neurons were different from each other, unlike the population bursts. While promising, we need to perform more experiments to confirm the results. The ultimate goal of our optogenetic stimulation of cultures is to recover the bursting patterns that we observe during spontaneous activity.

4.1 Conclusion

Bursts interrupting asynchronous dynamics in neural networks are population-wide neural events characterized by a large synchronous oscillation of all the cells in the network. Their generation is a consequence of a combination of network recurrent activity with a temporary imbalance of excitation and inhibition. We proved the burst duration and frequency are both strongly related to the network density and in general increase for higher densities. We provided strong evidence suggesting population bursts may be generated locally within a region where the E/I imbalance was broken and propagate like a wave throughout the entire network. The mechanisms responsible for the uncompensated excitation in these specific

regions are yet unknown, but cells located at or near that region must be somehow different to the others. Some hypothesis are that there may be an unusually lower number of inhibitory cells, that inhibitory synapses lose their efficiency or that inhibition becomes slower and is overtaken by excitation. We perform preliminary computer simulations below to elucidate possible mechanisms.

Chapter 5

The computational model

5.1 Motivation

Computer simulations are a popular way to model biological systems. Their starting point being the mere imitation of the experimental results, they ultimately aim to become a tool to predict the outputs of biological experiments. I modeled a recurrent network of coupled excitatory and inhibitory leaky integrate-and-fire neurons with conductance-based adaptive synapses and external inputs at the origin of the spiking activity. The aim is to produce the salient properties of the experimental results from the previous chapter. Further, computer simulations allow to test the effect of possible mechanisms for E/I imbalance in the network.

Simulations were programmed with Python, concretely with the packages `numpy, scipy, time, random` and `matplotlib`. Differential equations were integrated using a first order Euler algorithm with 0.01 ms as time step. Detailed codes of the simulations are included in Section S3 of the Supplementary material.

5.2 Single neuron model

I started with a model of a single LIF neuron receiving a variable number of E and I inputs. The total number of inputs, N, and the fraction of E inputs, r, are adjustable parameters. Spontaneous and stimulated activity of the neuron were inspected as a first approach to understand some of the mechanisms at the origin of spiking outputs and bursting behaviors.

5.2.1. Spontaneous activity of the LIF neuron

To reproduce spontaneous activity of neurons observed in experiments, a Gaussian unbiased noise current was injected to the cells. From the experiments, between 20 and 30% of the neurons fired spontaneously[2] (named SS) while the rest where silent (non-spiking or NS) but nevertheless received noisy inputs. For the model, the input noise into the NS neurons had a small

variance (Fig. 5.1A), while SS neurons received a larger one (Fig. 5.2B) that allowed for random occasional spiking.

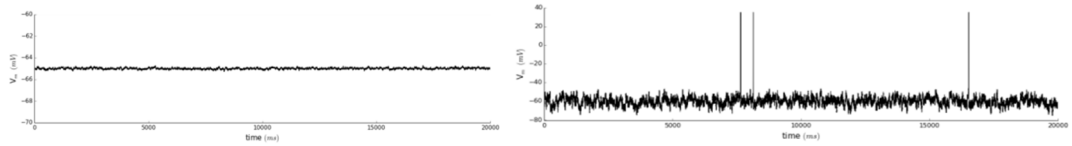

(A) (B)

Figure 5.1. Patterns of the spontaneous activity of a LIF neuron. A. Spontaneously non-spiking (NS) neuron receiving an unbiased input Gaussian current of 0.1 nA variance**. B.** Spontaneously spiking (SS) neuron receiving an unbiased input Gaussian current of 3.0 nA variance.

5.2.2. Stimulated activity of a single LIF neuron

Stimulating a single LIF with discrete inputs can open a window to understand the mechanisms underlying the formation of varying spiking patterns[43]. Inputs can either represent synaptic inputs or an external stimulation of the network. Random and correlated Poisson spike trains at a mean rate of 5Hz and varying ratio of E/I cells entered the LIF neuron (Fig. 5.2, left-hand column). Synaptic strength and time-to-peak values were taken from the data on cortical slices[22,28,29] without specifying the identity of the postsynaptic neuron.

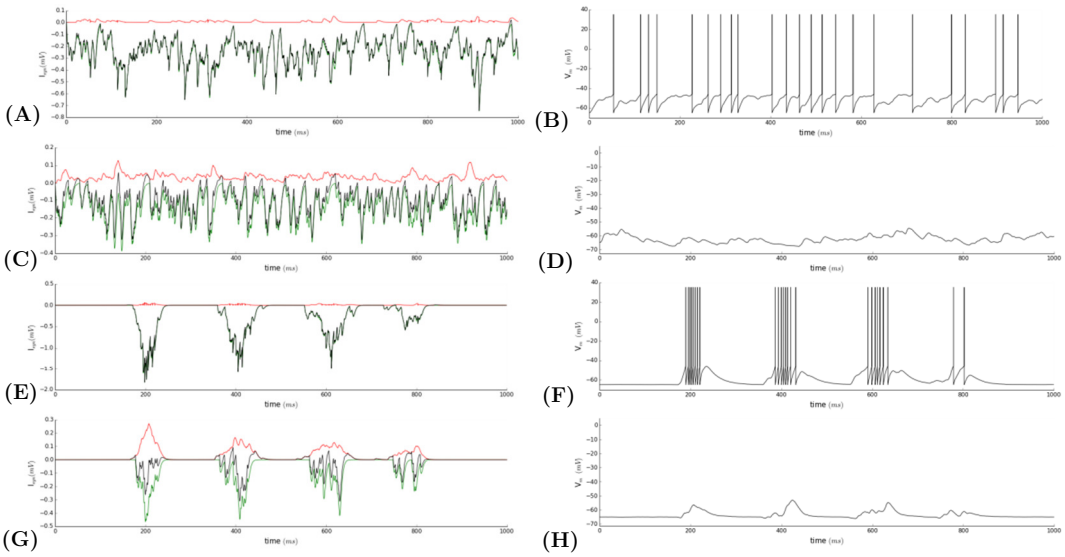

Figure 5.2. Evoked activity of a LIF neuron. A-D. Excitatory (green), inhibitory (red) and net (black) random synaptic input currents at a rate of 5 Hz into a NS neuron for N=100 inputs and a 90% (A) and 20% (C) of excitation and evoked potentials (b and D respectively). **E-H.** Same color code and E-I ratios than A and C, but for Poisson-like (λ=200 ms) correlated excitatory and inhibitory inputs and evoked potentials.

As expected, the more the net current is shifted towards excitation, the more probable for the neuron to spike. Roughly constant E and I inputs

(Fig. 5.2A, C) can either lead to regular spiking if the net current is high enough to drag the potential above threshold (Fig. 5.2B) or to a quiescent state if inhibition counterparts excitation (Fig. 5.2D). However, neither of those mechanisms lead to transient bursts of high firing rates. On the other hand, nearly synchronous E and I inputs (Fig. 5.2E, G) can lead to intermittent overriding of excitation upon inhibition that drives the membrane potentials over short periods of solid depolarization (Fig. 5.2F) if E is strong enough. Although these results seem predictable, they make a good and visible proof that the E-I imbalance leading to bursts must be temporarily bounded.

In the next section, we construct a full network so that the E/I inputs arise from the induced dynamics of the network rather than artificially specified as above.

5.3 Characteristics of the network

A thorough characterization of the neural network in *in vitro* cultures was conducted in Chapter 3. As this model tries to be as biologically accurate as possible without sacrificing speed (see discussion in Section 5.6), experimental results on the neuron's intrinsic and synaptic properties as well as the network's spatial distribution were replicated. All neurons have slightly different membrane resistance, time constant and threshold voltage that are normally distributed around the values obtained in Section 3.3.2. The mean threshold voltage is -46mV. The cultures' dimensions are 1.3mm × 1.3mm. The total number N of cells is obtained with the network density n, in cells/mm^2.

5.3.1. Clustered spatial distribution

Experimental results in Chapter 3 showed that the network's architecture tends to range from random to clustered depending on the density. One of the advantages of *in vitro* cultures is the thinness of the layer of cells. For simplicity, the network is considered 2-dimensional. The percentage of excitatory (r_e) and inhibitory (r_i) neurons belonging to clusters are two separate inputs to the subroutine, allowing to obtain a wide number of geometrical configurations. The total number of clusters is chosen randomly for each trial, so are the coordinates of their centers and the numbers of E and I neuron belonging to each one of them. E and I neurons are distributed sequentially in clusters (see Section S3.4 of the Supplementary

material). Finally, the resting neurons are placed randomly through the network. Boundary conditions are always applied.

One can obtain a wide range of geometrical distributions, from a uniformly distributed network (Fig. 5.3 A, D) to a totally clustered one (Fig. 5.3 B, E) by simply varying the values of r_e and r_i. The more realistic configuration is a balance of the two previous (Fig. 5.3 C, F), which is the one we used in most all the simulations.

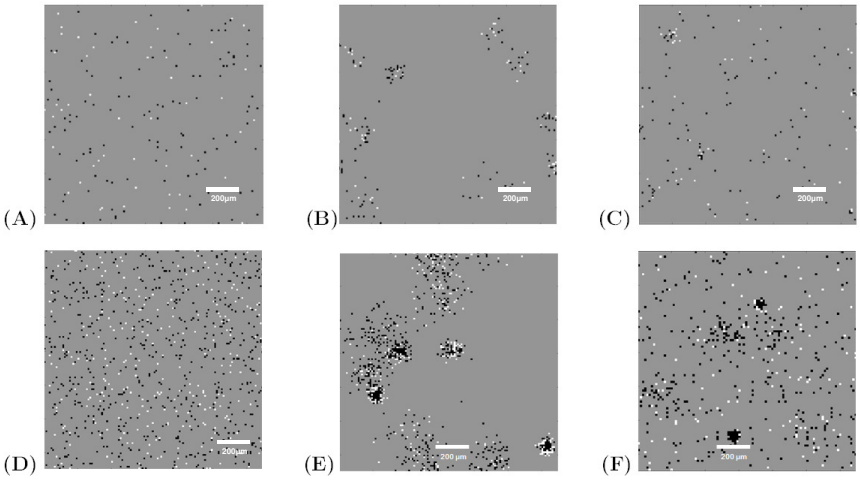

Fig. 5.3. Network geometries. All results are for a 40% of inhibitory neurons. Black dots represent excitatory neurons, white dots represent inhibitory ones. **A and D.** Completely random network distribution (r_e=r_i=*0*) for a sparse (n=*100* $\frac{cells}{mm^2}$) and a dense (n=*500* $\frac{cells}{mm^2}$) network. **B and E.** Completely clustered network distribution (r_e=r_i=*1*) for the same network densities than before. **C and F.** Equilibrated random and clustered network (r_e=*0.3* , r_i=*0.4*) for the same network densities.

5.3.2. Synaptic properties and connectivity

a) Connectivity profile

The non-symmetric connections between neurons are based on previous results on slices and cultures[2,22]. They model the connection probability as a Gaussian distribution decreasing with the distance with characteristic length around 600µm between neurons and peak probabilities that are specific to each type of synapse[2]. This profile is attributed to the connections between randomly distributed neurons, neurons in the same cluster or random neurons with neurons in clusters. However, the number of interconnected neurons between clusters is increased to favor the propagation of signals within these enclosed structures.

b) Heterogeneity of the coupling

Synaptic properties in the central nervous system can depend on an elevated number of parameters[33], such as the identity of the pre and postsynaptic neurons, their location or synaptic plasticity. The time courses of the conductance and the induced PSPs depend on the type of synapse (Fig. 5.4).

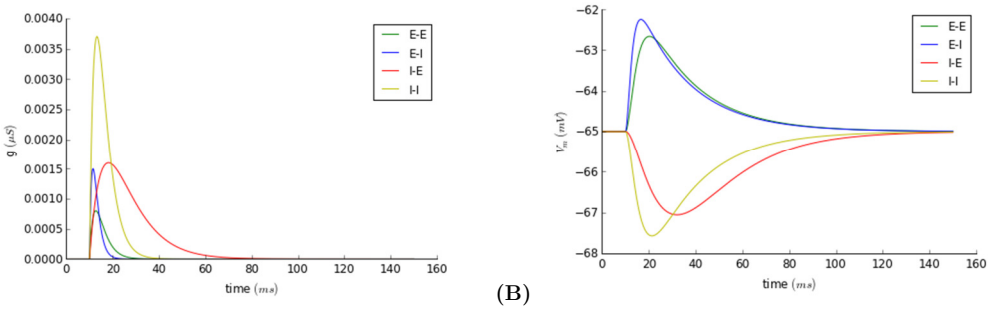

(A) (B)

Figure 5.4. Synaptic conductances and evoked PSPs. A. Postsynaptic conductance for the four types of couplings. **B**. Evoked excitatory and inhibitory postsynaptic potentials. Amplitude in mV and time to peak in ms of PSPs are (τ_{peak}=*10.1* ; V_{PSP}=*2.3*) for E-E, (τ_{peak}=*6.8* ; V_{PSP}=*2.7*) for E-I, (τ_{peak}=*21.8* ; V_{PSP}=*-2.1*) for I-E and (τ_{peak}=*12.6* ; V_{PSP}=*-2.6*) for I-I. Conductance parameters were chosen to get PSPs with the previous characteristic parameters for a neuron with R_m=*200MΩ* and τ_m=*22 ms*. Values for the amplitude and time-to-peak of PSPs were taken from unpublished research of the Reyes group[2].

c) Short-term synaptic depression

Synaptic fatigue is an indispensable feature of synaptic plasticity for the generation of stable population bursts, as it is thought to be a form of negative feedback to overwhelming synaptic activity. Short-term synaptic depression (STD) denotes the changes in synaptic efficiency depending on the firing history of the neuron (see Section 3.2.2). STD is attributed to the depletion of the readily releasable vesicles after synaptic activity. Its electrophysiological implication is a decrease in the synaptic strength that recovers after a delay that depends on the type of neuron. The effective synaptic conductance that accounts for STD is obtained as a product with a defined *synaptic variable*. The latter is maximum and unitary when the neuron is fully active and is reduced by a 30% whenever the neuron spikes. Recovery is exponential (eq. 5.1) with a characteristic time constant that depends on the type of neuron. Fig. 5.5A and B show the synaptic variables associated to two example excitatory and inhibitory neurons firing synchronously.

$$\frac{1}{\tau_j}\frac{dI_{syn}}{dt} = 1 - I_{syn} \qquad , \qquad j=\{e,i\} \tag{5.1}$$

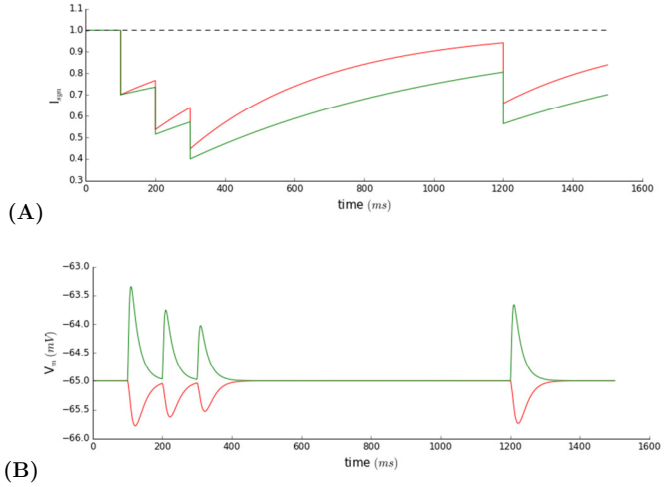

Figure 5.5. Short-term synaptic depression. (Synchronized) Spike times correspond to instants where a dramatic decrease in I_{syn} is noticeable. **A.** Synaptic variable of an excitatory (green) and an inhibitory (red) presynaptic neuron. **B.** Evoked EPSP (green) and IPSP (red). STD is obvious from the changes in the amplitudes of successive PSPs. The original shape is yet not recovered even 0.9 s after the last spike in the initial triplet. The time constant of depression is 400ms for I and 800ms for E, according to data on neural cultures[2].

5.4 Analysis of the spontaneous activity

The spontaneous activity of the network was generated as described in Section 5.2.1. SS neurons are chosen randomly by picking an adjustable percentage of E neurons within a region that is selected with an interactive window. We will call that region the overexcited area (OA; often a cluster) that represents the "hotspot" we described in Section 4.4. The rest of the cells are NS. We tested the effect that network density (for a particular connectivity profile) and the architecture have on the emergence of synchronous dynamics. The first 250ms of simulations are usually cut-off as it is where the transient occurs and artificial onset effects often appear.

5.4.1. Dependence on the network density

The model exhibits similar behaviors as the experiments: no bursts are observed for lower densities (Fig. 5.6A) and one appears when the network is denser (Fig. 5.6C). Both networks exhibit periods of quiescence, during which only the SS fire asynchronously approximately following Poisson-like statistics (Fig. 5.6B). For the highest density, this long period is interrupted by a population burst that lasts about 20ms and involves all the cells in the network (red star).

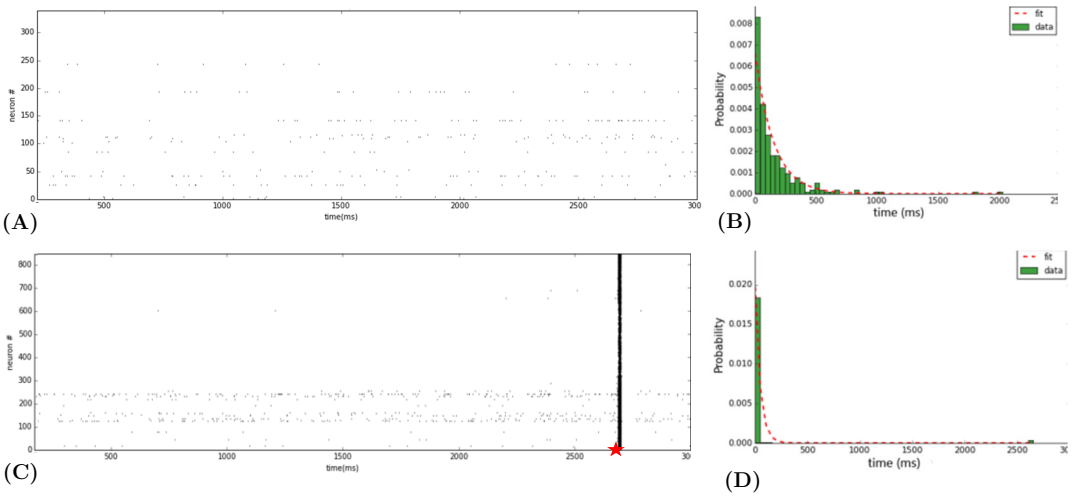

Figure 5.6. Dependence of bursting dynamics on network density. A. Raster plot of the network activity for a network of 200cells/mm^2. The neuron number is in the y-axis and dots represent firing times for each neuron. **B**. Exponential interspike interval (ISI) distribution with parameter λ=*0.007ms^{-1}* for the network in A, that proves the spike times are Poisson-like variables. **C**. Raster plot for a network of 500 cells/mm^2. The red star indicates the beginning of the burst. **D**. ISI distribution for the network in C. It cannot be fit with an exponential because of the prominent peak at 0, consequence of the burst.

5.4.2. Role of the architecture

The architecture of both networks is depicted in Fig. 5.7A and C. The configuration is set so as to make sure that 70% of the E and 20% of the I neurons in clusters are connected to each other. The "hotspot" is surrounded by other neurons and clusters in both cases. Neurons in the hotspot are driven by the same spontaneous dynamics. However, in one case only SS fire (Fig. 5.7B) while the architecture of the second one and the greater number of SS neurons allows for the burst to start and to be propagated. From Fig. 5.7D, we can see all neurons are activated and that it is the ones in clustered structures that fire the most (apart from the ones in the OA).

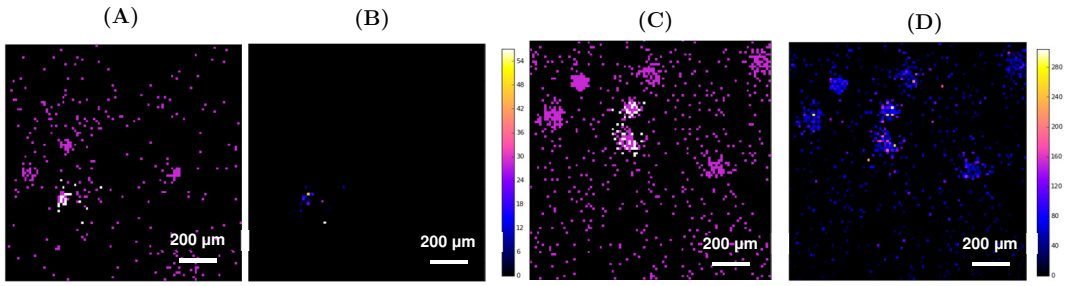

Figure 5.7. Spatial structure and spike count. A. NS neurons (pink) and SS ones (white) in the network of 200 cells/mm^2. **B**. Active neurons and number of spikes. **C**. Same than A but for 500cells/mm^2. **D**. Active neurons and number of spikes. All neurons in the network are active (it happens during the burst) and neurons in clusters fire more vigorously.

4.2.3. Dynamics at the 'hotspot'

When taking a closer look at the spiking patterns of the SS neurons in the OA (Fig. 5.8A), neurons fire spontaneously until they get synchronized for some reason and generate the population burst (red star) followed by a period of complete quiescence. To check that this happened stochastically and not systematically, two other simulation were run and only one of them exhibited a burst. One can see by comparing the timing in Fig. 5.8 and B that the burst starts slightly later in the NS neurons than in the SS. This confirms the burst is generated within the OA and then propagates to the rest of the network. This can also be deducted from the low subthreshold activity of the NS neurons.

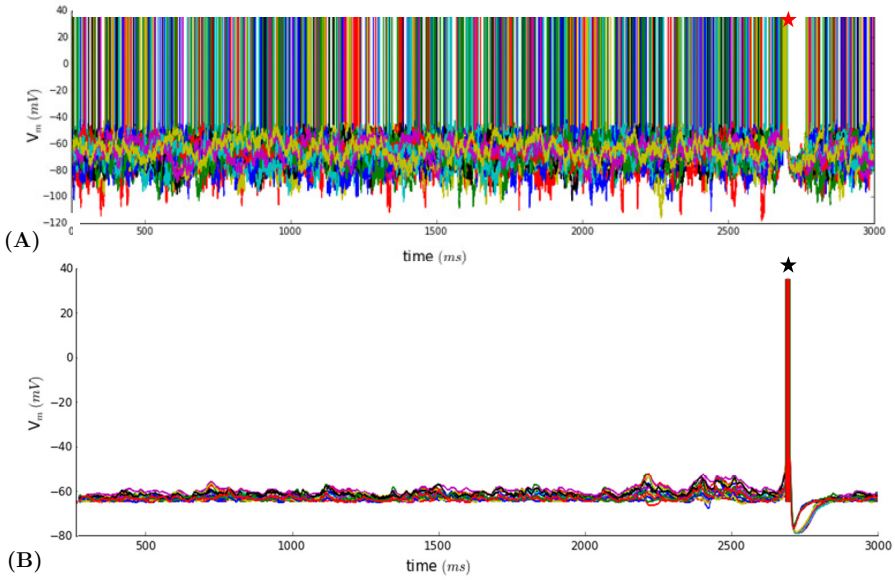

Figure 5.8. Dynamics of the 'hotspot' and the rest of the neurons. A. Dynamics of all of the SS neurons in the OA. **B**. Dynamics of a few NS neurons.

These results suggest two things. First, a "hotspot" containing a number of spontaneously firing excitatory neurons can generate population burst. Neurons within that region exhibit random (probably Poisson-like) spiking times and get, sometimes and somehow, synchronized to produce the burst that is afterwards propagated to the rest of the cells. Secondly, these dynamics are possible in clustered networks provided they are dense enough so as to have architectures that enable the propagation of the bursts. More enigmatic is the fact that bursts are not generated (not even in the OA) for lower densities. This may be due to the fact that less neurons were SS, or that the cluster was too small to get to synchronize their dynamics.

What follows is to test whether population bursts can be reproduced during stimulated activity that mimics photostimulation of our *in vitro* cultures.

5.5 Analysis of the stimulated activity

5.5.1. Shape of the stimulus

We stimulate the network with uncorrelated Poisson spike trains at a rate of approximately 7Hz (Fig. 5.9B). The stimulus starts at *t=500ms* and lasts for 5s (see Section S3.6 of the Supplementary material). Random E and I neurons are stimulated within a region of interest (named ROI; Fig. 5.9A) that can be defined in an interactive Python window.

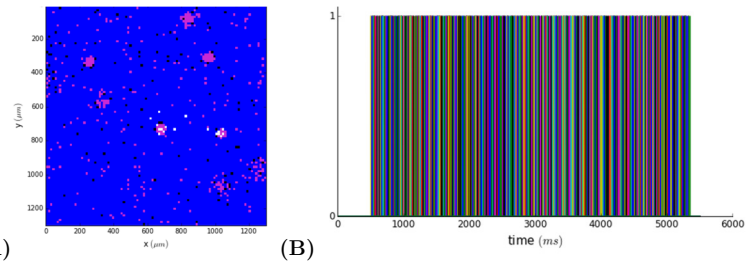

Figure 5.9. Photostimulation of the computational network. A. Random E and I neurons are stimulated within a region of interest. E cells are pink, I cells are black and stimulated E and I cells are white**. B**. Superposition of all the train pulses driving the cells in A. Pearson coefficients of different pulse trains are of the order of 10^{-5}, thus they can be considered completely uncorrelated.

5.5.2. Stimulated activity in a network without an OA

First, we stimulate a network where no OA has been defined, meaning neurons do not fire spontaneously and membrane potentials only show small variations due to their noise current. One can see in Fig. 5.10 A and B that the stimulus starting at *t=500ms* (black arrow) is not strong enough so as to drive the neurons over their threshold.

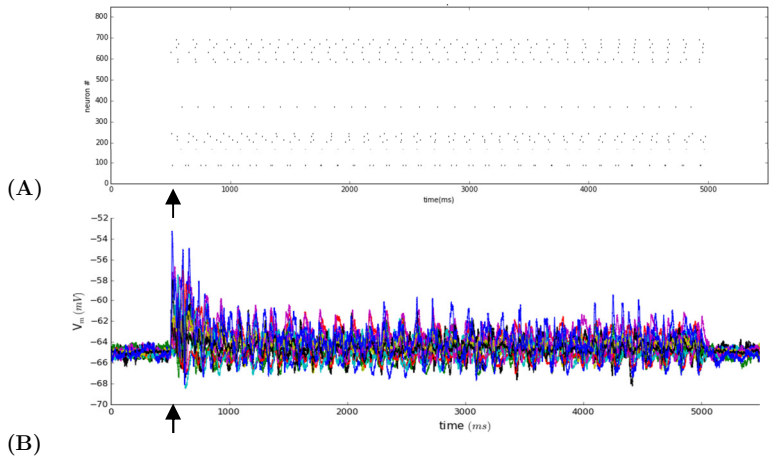

Figure 5.10. Evoked membrane potentials in a network without OA. A. Raster plot of the network. Only the stimulated neurons fire at the times they are stimulated. **B**. Dynamics of the membrane potentials of some NS neurons in the network. EPSPs are visible but do not reach threshold. Black arrows indicate the beginning of the stimulus.

5.5.2. Stimulated activity in a network with an OA

Then, we stimulate a network where a "hotspot" has SS neurons. The region of interest is different than the OA to separate the effect of the two spiking mechanisms (white and orange spots in Fig. 5.12A). In this case, the beginning of the stimulus (black arrows) triggers a burst that is most probably due to onset effects. This is followed by five more population-wide burst oscillations (red stars) that arise from the synchronization of the SS. Note that, in this case, the stimulated neurons are not in the OA but they still have an effect on their synchronization. Unless bursts in Fig. 5.11A are by any chance only due to the spontaneous activity of the SS neurons, it seems the external stimulation can act as a synchronization mechanism. More simulations should be run to confirm this outcome.

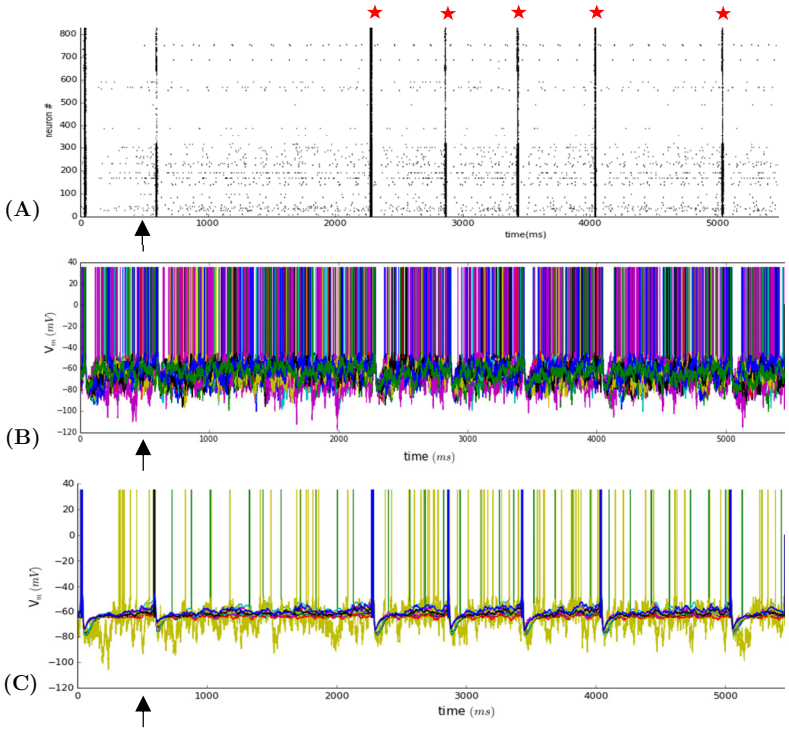

Figure 5.11. Evoked membrane potentials in a network with OA. A. Raster plot of network activity**. B**. Dynamics of the SS neurons in the OA. They fire spontaneously and are suddenly synchronized after the stimulus. **C.** Dynamics of several neurons. The yellow neuron is SS, the blue and red cells are stimulated and the rest are neither stimulated or SS. Red stars represent population bursts that are not due to onset effects.

As for the activation of the network, all neurons are activated during these bursts, but, again, it is the ones that are in clusters that fire the most. OA and ROI are as far from each other as possible (Fig. 5.12A) and still, the one feels the effect of the other. This is, of course, because they both contain clusters that are connected to each other.

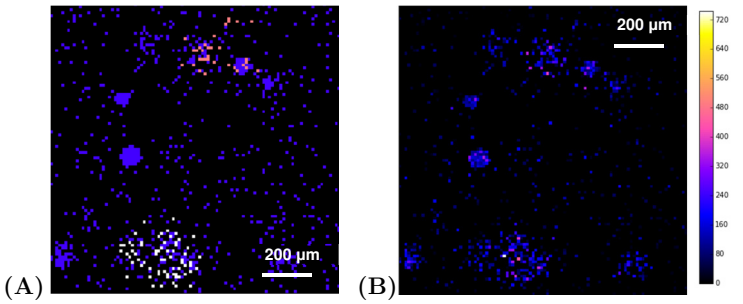

Figure 5.12. ROI, OA and network activity. A. Stimulated (orange), SS (white) and NS (blue) neurons. **B**. Active neurons and spike count.

Our second analysis of the network model proved that an external excitation is not enough to generate population bursts unless there already is an existing noisy activity within it. We managed to stimulate a ROI separated from the OA and still appreciate the emergence of these population-wide neural events.

5.6 Conclusion

Building a computer model of a network of LIF neurons allowed us to test some mechanisms for breaking the E-I balance that we could not investigate with the experiments (yet).

First, a simpler model of a single neuron receiving a large number of inputs showed that transient epochs of excessive excitation lead to bursting patterns. Then, we analyzed the spontaneous activity of an entire network of E and I neurons where a "hotspot" containing a few number of excitatory neurons that fired spontaneously. Whereas low densities did not favor the generation of population bursts and interspike intervals remained Poisson-like, higher densities produced an architecture that allowed bursts to emerge and to be propagated. SS neurons fired randomly for most of the simulation until, somehow, they synchronized their activity and by that produced an excess of excitatory activity that activated population burst. Finally, we studied the effect of stimulation on the network by occasionally activating some cells within a region of interest (ROI) with Poisson pulse trains. The stimulus did not trigger any population bursts when the network did not have a hotspot, while several synchronous events happened when there was one.

Unfortunately, our model has some limitations. First, LIF neurons are the simplest model and have imperfect biological realism while being optimal for large-scale networks simulations. Still, the computation time of the simulations is too long and would have to be lowered in an enhanced version

of the program. Also, the population bursts that we get are too short compared to the experimental results: they last around 20 ms while those characterized in Chapter 4 lasted on average 1s. Finally, the model does not take into account many properties that would most probably give rise to other spike patterns. For example, we considered the synaptic depression of E and I to be equal in amplitude. The connections between clusters are also unrealistic as they were set to be particularly probable to enhance the effect of this architecture.

Final discussion

The combination of analyses on electrophysiological recordings in cultures of live neurons and computer simulations allowed us to study the characteristics of population-wide bursts in neural networks and gave us an insight into E-I imbalanced dynamics.

The preparation of *in vitro* cultures of cortical neurons and patch clamp techniques allowed to, first, document the characteristics of the cultures. We found neurons' intrinsic properties that are comparable to previous measurements on cortical slices[22,28,29]. As for the geometry, dense networks were found to be organized in groups of clusters. Theoretical studies[23] and our computer model suggest these structures are a key feature of neural network for the emergence of states of collective synchronous activity. As these are only early results, we should run more simulations where the architecture and connectivity profile of the network would vary in order to appreciate their effect on the emergence of population bursts. Finally, besides from recovering a connectivity profile that is in agreement with previous experiments[22], we showed that short-term synaptic depression seems more important for inhibition than for excitation. Again, this could be a mechanism for breaking the E-I balance and the simulations could provide the perfect tool to test it.

A thorough analysis of electrophysiological data followed. First, we confirmed that population bursts emerge due to network activity and not within a single cell, as strongly correlated oscillations of the membrane potentials are recorded simultaneously in all the neurons. Then, by studying cultures of different densities, we were able to determine that the frequency and duration of the bursts are strongly related to this parameter, confirming one of our initial hypothesis. Indeed, low densities, thus low recurrent network activity, are not enough to generate collective events. It is in denser networks that population bursts interrupt asynchronous dynamics.

Moreover, a rigorous inspection of recorded voltage traces suggests that bursts may be generated at a "hotspot" and then propagated like a wave through the network. We hypothesize that cells within that specific region must somehow be different than the others in order for an E/I imbalance to appear. As a first endeavor to test this conjecture, we were able to run some simulations in which an enclosed region of the network stood out from the others for having a number of excitatory neurons that fired spontaneously. When the network was clustered and dense enough, these neurons that usually spiked in random patterns somehow coordinated their activities and

generated one or more population bursts. The stochasticity of their synchronization could actually be reproducing what is happening in the cultures. What comes next is to associate this overwhelming excitability that in the model is represented by nearby cells firing spontaneously with properties that can be measured on real neurons in the cultures.

Finally, we have made a first attempt to study the effects of external stimulation on evoked network dynamics. The experimental approach was to use optogenetic techniques to stimulate a number of ChR2-expressing neurons with spatiotemporally accurate pulses. Apparently, results support the idea of a spatial heterogeneity of neural and synaptic properties being at the origin of population bursts, as no collective events emerged when we illuminated a random area of the network. On the other hand, in the model, the stimulation of a region of interest differing from the "hotspot" seemed to have an effect on triggering the synchronization of the spontaneous firing within that region and recover the population bursts.

This short yet promising work is the outset of a wider project that will be a collaboration between the Reyes group and another laboratory. Some of the hypothesis they made on burst frequency and origin were confirmed in this early version. However, more data has to be collected to confirm and determine all the dependences that we found in this project. Now, further research aims to: 1) narrow the location of the "hotspot" via patch clamp and optogenetic techniques; 2) reveal the properties that make neurons within this area be different than the rest of the culture; 3) improve and extend the computer simulation so as to sort out its actual limitations and achieve to elucidate more mechanisms for the E/I imbalance. These studies will lead to a better understanding of network processing as well as elucidating the processes that lead to neuropathologies.

References

1. Angstadt JD, Grassman JL, Theriault KM, Levasseur SM (2005) Mechanisms of postinhibitory rebound and its modulation by serotonin in excitatory swim motor neurons of the medicinal leech. *Journal of Comparative Physiology.* 191(8): 715-732
2. Barral J, Reyes A (2016) Scaling of synaptic strength with network size: effects on excitatory/inhibitory balance and neural dynamics. *Unpublished.*
3. Barranca V. J , Johnson D. C, Moyher J. L, Sauppe J. P, Shkarayev M. S, Kovacic G, Cai D (2014) Dynamics of the exponential integrate-and-fire model with slow currents and adaptation. *Journal of Computational Neuroscience.* 37(1): 161-180
4. Benayoun M, Cowan J.D, Van Drogelen W, Wallace E (2010) Avalanches in a stochastic model of spiking neurons. *PLOS Computational Biology.* 6 (7)
5. Bressloff P C (2010) Metastable states and quasicycles in a stochastic Wilson-Cowan model of neuronal population dynamics. *The American Physical Society.* 82
6. Bromfield EB, Cavazos JE, Sirven JI (2006) An introduction to epilsepsy, Chapter 1: Basic mechanisms underlying seizures and epilepsy. *American Epilepsy Society*
7. Diesmann M, Gewalting MO, Aetsen A (1999) Stable propagation of synchronous spiking in cortical neural networks. *Nature.* 402: 529-533
8. Ecker A.S, Berens P, Keliris G.A, Bethge M, Logothetis N.K, Tolis A.S (2010) Decorrelated neuronal firing in cortical microcircuits. *Science.* 327:584-587
9. Fain GL (1999) Molecular and cellular physiology of neurons. Cambridge, Massachussets. *Harvard University Press.*
10. Gentet L.J, Avermann M, Matyas F, Staigner J.F, Petersen C.C.H (2010) Membrane potential dynamics of GABAergic neurons in the barrel cortex of behaving mice. *Neuron.* 65:422-435
11. Graupner M, Reyes A.D (2013) Synaptic input correlations leading to membrane potential decorrelation of spontaneous activity in cortex. *The Journal of Neuroscience.* 33(38): 15075-1508
12. Grienberger C, Konnerth A (2012) Imaging calcium in neurons. *Neuron.* 73: 862-885
13. Häusser M, Roth A (1997) Estimating the time course of the excitatory synaptic conductance in neocortical pyramidal cells using a novel voltage jump method. *The Journal of Neuroscience.* 17(20): 7606-7625

14. Heeger D (2000) Poisson model of spike generation. *Lecture at the CNS, NYU.*
15. Heiss J, Katz Y, Ganmor E, Lampl I (2008) Shift in the balance betwwen excitation and inhibition during sensory adaptation of S1 neurons. *The Journal of Neuroscience.* 28(49): 13320-13330
16. Henning M. H .Modelling Synaptic Transmission. University of Edinburgh.
17. Hodgkin A L, Huxley A. F. (1952) A quantitative description of membrane current and its application to conduction and excitation in nerve. *The Journal of Physiology.* 117(4): 500-544
18. Izhikevich E M (2003) Simple model of spiking neurons. *IEEE Transactions of Neural Networks.* 14(6): 1569-1573
19. Jia Q, Chen Z (2011) Coupled network synchronization of non-identical Hindmarsh-Rose model. *Proceedings of June 2011 International Conference on Modelling, Identification and Control, Shanghai, China.*
20. Johnston D, Wu SM (1997) Foundations of cellular neurophysiology. Cambridge, Massachussets. London, England. *The MIT Press*
21. Levitan IB, Kaczmarek LK (1997) The neuron. New York. *Oxford University Press.*
22. Levy RB, Reyes AD (2012) Spatial profile of excitatory and inhibitory synaptic connectivity in mouse primary auditory cortex. *The Journal of Neuroscience.* 32(16): 5609-5619
23. Litwin-Kumar A, Doiron B (2012) Slow dynamics and high variability in balanced cortical networks with clustered connections. *Nature Neuroscience.* 15(11):1498-1508
24. Luczak A, Barthó P, Harris K.D (2009) Spontaneous events outline the realm of possible sensory responses in neocortical populations. *Neuron.* 62: 413-425
25. Magee J C (2000) Dendritic integration of excitatory synaptic input. *Neuroscience.* 1: 181-190
26. Naud R, Marcille N, Clopath C, Gerstner W (2008) Firing patterns in the adaptive exponential integrate-and-fire model. *Biological Cybernetics.* 99:335-347
27. Okun M, Lampl I (2008) Instantaneous correlation of excitation and inhibition during ongoing and sensory-evoked activities. Nature Neuroscience. 11(5): 535-537
28. Oswald AM, Reyes AD (2011) Development of inhibitory timescales in auditory cortex. *Cerebral Cortex.* 21:1351-1361
29. Oswald AM, Reyes AD (2008) Maturation of intrinsic and synaptic properties of layer 2/3 pyramidal neurons in mouse auditory cortex. *J. Neurophysiol.* 99: 2998-3008

30. Perkins KL (2006) Cell-attached voltage-clamp and current-clamp recording and stimulation techniques in brain slices. *J. Neurosci Methods*. 54: 1-18
31. Renart A, De la Rocha J, Bartho P, Hollender L, Parga N, Reyes AD, Harris KD (2010) The asynchronous state in cortical circuits. *Science*. 327: 587-590
32. Richardson M.J.E. , Gerstner W. Conductance versus current-based integrate-and-fire neurons: is there qualitatively new behavior? *Lausanne lecture.*
33. Roth A, Van Rossum M (2009) Computational modeling methods for neuroscientist (Chapter 6: Modeling synapses). *The MIT Press.*
34. Sakmann B, Neher E (1984) Patch clamp techniques for studying ionic channels in excitable membranes. *Ann. Rev. Physiol*. 46: 455-472
35. Schneidman E, Berry M.J, Segev R, Bialek W (2006) Weak pariwise correlations imply strongly correlated network states in a neural population. *Nature*. 440: 1007-2012.
36. Shu Y, Hasenstaub A, McCormick DA (2003) Turning on and off recurrent balanced cortical activity. *Nature*. 423: 288-293
37. Tuckwell H. C (1988) Introduction to theoretical neurobiology, Volume 2. *Cambridge University Press.*
38. Tsodyks M, Kenet T, Grinvald A, Arieli A (1999) Linking spontaneous activity of single cortical neurons and the underlying functional architecture. *Science*. 283: 1943-1946
39. Van Vreeswijk C, Sompolinsky H (1996) Chaos in neuronal networks with balanced excitatory and inhibitory activity. *Science*. 274: 1724-1726
40. Veitinger S (2011) The patch-clamp technique – an introduction. *Science Lab*
41. Wells R.B. Biological signal processing (Chapter 3: The Hodgkin-Huxley model).
42. Wilson CJ (2013) Active decorrelation in the basal ganglia. *Neuroscience.* 250: 467-482
43. Yim M Y, Kumar A, Aertsen A, Rotter S (2014) Impact of correlated inputs to neurons: modeling observations from *in vivo* intracellular recordings. *The Journal of Computational Neuroscience*. 37(2): 293-304